NASA/TP–2012-217363

Paramyxovirus Infection Mimics *In Vivo Cellular Dynamics* in Three-Dimensional Human Bronchio-Epithelial Tissue-Like Assemblies

Anne M. Deatly[2]
Yen-Huei Lin[2]
Maureen McCarthy[1]
Wei Chen[2]
Lynn Z. Miller[2]
Jorge Quiroz[3]
Becky M. Nowak[2]
Robert A. Lerch[2]
Stephen A. Udem[2]
Thomas J. Goodwin[1]*

[1] *Disease Modeling and Tissue Analogues Laboratory, NASA Johnson Space Center, Houston, Texas 77058*
[2] *Vaccines Discovery, Wyeth Research, Pearl River, New York 10965*
[3] *Biometrics Research, Wyeth Research, Pearl River, New York 10965*

**Correspondence should be addressed to: Disease Modeling and Tissue Analogues Laboratory, NASA Johnson Space Center, Houston Texas, 77058*

August 2012

THE NASA STI PROGRAM OFFICE . . . IN PROFILE

Since its founding, NASA has been dedicated to the advancement of aeronautics and space science. The NASA Scientific and Technical Information (STI) Program Office plays a key part in helping NASA maintain this important role.

The NASA STI Program Office is operated by Langley Research Center, the lead center for NASA's scientific and technical information. The NASA STI Program Office provides access to the NASA STI Database, the largest collection of aeronautical and space science STI in the world. The Program Office is also NASA's institutional mechanism for disseminating the results of its research and development activities. These results are published by NASA in the NASA STI Report Series, which includes the following report types:

- TECHNICAL PUBLICATION. Reports of completed research or a major significant phase of research that present the results of NASA programs and include extensive data or theoretical analysis. Includes compilations of significant scientific and technical data and information deemed to be of continuing reference value. NASA's counterpart of peer-reviewed formal professional papers but has less stringent limitations on manuscript length and extent of graphic presentations.

- TECHNICAL MEMORANDUM. Scientific and technical findings that are preliminary or of specialized interest, e.g., quick release reports, working papers, and bibliographies that contain minimal annotation. Does not contain extensive analysis.

- CONTRACTOR REPORT. Scientific and technical findings by NASA-sponsored contractors and grantees.

- CONFERENCE PUBLICATION. Collected papers from scientific and technical conferences, symposia, seminars, or other meetings sponsored or cosponsored by NASA.

- SPECIAL PUBLICATION. Scientific, technical, or historical information from NASA programs, projects, and mission, often concerned with subjects having substantial public interest.

- TECHNICAL TRANSLATION. English-language translations of foreign scientific and technical material pertinent to NASA's mission.

Specialized services that complement the STI Program Office's diverse offerings include creating custom thesauri, building customized databases, organizing and publishing research results . . . even providing videos.

For more information about the NASA STI Program Office, see the following:

- Access the NASA STI Program Home Page at http://www.sti.nasa.gov

- E-mail your question via the internet to help@sti.nasa.gov

- Fax your question to the NASA Access Help Desk at (301) 621-0134

- Telephone the NASA Access Help Desk at (301) 621-0390

- Write to:
  NASA Access Help Desk
  NASA Center for AeroSpace Information
  7115 Standard
  Hanover, MD 21076-1320

NASA/TP–2012-217363

Paramyxovirus Infection Mimics *In Vivo Cellular Dynamics* in Three-Dimensional Human Bronchio-Epithelial Tissue-Like Assemblies

Anne M. Deatly[2]
Yen-Huei Lin[2]
Maureen McCarthy[1]
Wei Chen[2]
Lynn Z. Miller[2]
Jorge Quiroz[3]
Becky M. Nowak[2]
Robert A. Lerch[2]
Stephen A. Udem[2]
Thomas J. Goodwin[1]*

[1] *Disease Modeling and Tissue Analogues Laboratory, NASA Johnson Space Center, Houston, Texas 77058*
[2] *Vaccines Discovery, Wyeth Research, Pearl River, New York 10965*
[3] *Biometrics Research, Wyeth Research, Pearl River, New York 10965*

**Correspondence should be addressed to: Disease Modeling and Tissue Analogues Laboratory, NASA Johnson Space Center, Houston Texas, 77058*

August 2012

Available from:

NASA Center for AeroSpace Information
7115 Standard Drive
Hanover, MD 21076-1320
301-621-0390

National Technical Information Service
5285 Port Royal Road
Springfield, VA 22161
703-605-6000

This report is also available in electronic form at http://ston.jsc.nasa.gov/collections/TRS/

Acronyms

ANOVA	analysis of variance
bPIV3 SF	Bovine PIV3 Shipping Fever
cp	cold passage
ds	double-stranded
EMA	epithelial membrane antigen
FDR	false discovery rate
HBE	human bronchio-epithelial
HBTC	human bronchi and trachea
hr	host-range
HRE	human respiratory epithelium
MAP2	microtubule associated protein 2
MIP-1α	Macrophage Inhibitory Factor 1-α
MOI	multiplicity of infection
pi	post infection
PVA	polyvinyl alcohol
PIV3	parainfluenza virus type 3
RANTES	Regulated upon Activation, Normal T cell-Expressed and -Secreted
RE	restriction enzyme
RSV	respiratory syncytial virus
RWV	rotating wall vessel
3D	three-dimensional
2D	two-dimensional
ts	temperature sensitive
TLA	tissue-like assembly
UV	ultraviolet
wt	wild type

Table of Contents

Abstract

Respiratory syncytial virus (RSV) and parainfluenza virus cause severe respiratory disease, especially in infants, children, and the elderly. An *in vitro* model that accurately mimics infection of the human respiratory epithelium (HRE) would facilitate vaccine development greatly. Monolayer cultures traditionally used to study these viruses do not accurately and precisely differentiate the replication efficiencies of wild type and attenuated viruses. Therefore, we engineered novel three-dimensional (3D) tissue-like assemblies (TLAs) of human bronchio-epithelial (HBE) cells to produce a more physiologically relevant *in vitro* model of the HRE. TLAs resemble HRE structurally and by expression of differentiated epithelial cell markers. Most significantly, wild type viruses exhibited a clear growth advantage over attenuated strains in TLAs unlike monolayer cultures**.** In addition, the TLAs responded to virus infection by secreting pro-inflammatory mediators similar to the respiratory epithelia of infected children. These characteristics make the TLA model a valuable platform technology to develop and evaluate live, attenuated respiratory virus vaccine candidates for human use.

Respiratory virus diseases, the most frequent and least preventable of all infectious diseases, range in severity from the common cold to severe bronchiolitis and pneumonia.[1, 2] Two paramyxoviruses, RSV and parainfluenza virus type 3 (PIV3), are responsible for a majority of the most severe respiratory diseases of infants and young children.[3] RSV causes 70% of all bronchiolitis cases[4] and is a major cause of morbidity and mortality worldwide, especially in infants.[5] PIV3 causes 10% -15% of bronchiolitis and pneumonia during infancy, second only to RSV,[6] and 40% of croup in infants.[7]

To date, licensed vaccines are not available to prevent these respiratory diseases. At present, traditional monkey kidney (Vero and LLC-MK2) and human (HEp-2) tissue culture cells and small animal models (mouse, cotton rat, guinea pig, ferret, and hamster) fail to accurately imitate viral replication and human disease states.[8] Lacking an authentic model has impeded the development and evaluation of live, attenuated vaccine candidates.

Development of a physiologically relevant *in vitro* tissue culture model that reproduces characteristics of the HRE, the primary target of RSV and PIV3, would aid in predicting clinical attenuation and safety of vaccine candidates. Successful tissue engineering of a 3D human intestinal model using novel NASA technology[9] inspired the development of a tri-culture 3D model for the HRE. Sequential layering of primary mesenchymal cells (comprised of normal human fibroblasts and endothelial cells) followed by BEAS-2B epithelial cells derived from

human bronchi and tracheae were recapitulated on Cultisphere and/or cytodex3 microcarriers in cylindrical vessels that rotate horizontally, creating an organized epithelial structure. Horizontal rotation randomizes the gravity vector modeling aspects of microgravity.[9,10] Mesenchymal and epithelial cells grown under these conditions reproduce the structural organization, multicellular complexity, and differentiation state of the HRE (Goodwin et al, NASA/TP 2008-214771).

The opportunity to study respiratory viruses in a nasal epithelium model is invaluable because the most promising respiratory virus vaccine candidates are live attenuated viruses for intranasal administration. Here we characterize the interactions of respiratory viruses and epithelial cells grown under modeled microgravity in comparison to gravity-ladened monolayers. 3D HBE TLAs and traditional monolayers (two-dimensional [2D]) are infected at 35°C, the upper temperature of the upper HRE,[11] to simulate *in vivo* infection conditions. Growth kinetics of wild type (*wt*) RSV and PIV3 viruses were compared in 2D and 3D cells to that of strains attenuated in humans[12-14] or rhesus macaques.[15]

This novel 3D HBE model also offers an opportunity to study whether the epithelial cell function, especially in host defense, is recapitulated by mimicking the structural organization of the HRE. *In vivo,* airway epithelial cells play a significant and dynamic role in host defense[16] by blocking paracellular permeability and modulating airway function through cellular interactions or tight junctions. As regulators of the innate immune response, epithelial cells constitutively express cytokines, chemokines, and colony-stimulating factors including RANTES, IL-8, IL-6, GM-CSF, and G-CSF for proactive host defense.[17] In response to viral infection, epithelial cells induce potent immuno-modulatory and pro-inflammatory cytokines that recruit phagocytic and inflammatory cells to clear the virus and enhance protection.

Although disease pathogenesis is classically attributed to the cytopathic effects of the pathogen, severe disease states associated with RSV and PIV3 are attributed to the inflammatory response, especially in infants. RSV is a potent inducer of cytokines and pro-inflammatory mediators in epithelial cells *in vivo*.[18] A differentiated human epithelial model independent of the complete functional immune system will help elucidate the role of epithelial cells in respiratory disease.

We reported here, virus and host cell interactions in 3D HBE TLAs are similar to those *in vivo*. Because the epithelial cell organization[19] of the TLAs impacts not only the expression of airway epithelial characteristics, but also cellular communication, the TLAs represent a more physiologically relevant model of the HRE than BEAS-2B or other non-tumour monolayer

models of respiratory disease. As a result, wild type respiratory viruses have a clear growth advantage over attenuated viruses in TLAs unlike traditional monolayers. In addition, the TLAs respond to wild type virus infection by secreting pro-inflammatory mediators characteristic of infected HRE. TLAs expressing microbial defense mechanisms provide an excellent model to study the interactions of respiratory pathogens with their host and to identify the innate immunity mediators. Therefore, 3D HBE TLAs offer advantages for the study of respiratory viruses and the development of viral vaccine candidates.

1.0 Results

Characterization of 3D HBE TLAs

The HBE-TLA is a multilayered tissue primarily comprised of pseudo-stratified epithelial cells, a basement membrane, and underlying mesenchymal cells.[16] Ciliated, secretory, and basal epithelial cells are joined by intercellular junctions and anchored to the basement membrane via desmosomal interactions. Through tight junctions and the mucociliary layer, the basement membrane maintains polarity of the epithelium and presents a physical barrier between the mesenchymal layer and the airway.[20,21]

To mimic the structural organization of the HRE, primary mesenchymal cells derived from human bronchi and tracheae (HBTC) form the initial layers of the TLAs on cytodex or Cultisphere microcarriers. Four to 6 days later, immortalized human epithelial BEAS-2B cells are layered on top**.** HBE TLAs develop in rotating wall vessels, a modeled microgravity environment (Fig. 1a–b). HBE TLAs share many of the structural and morphological characteristics of the HRE including multiple layers (Fig. 1c-f) of different cell types as indicated by different shapes of cells and nuclei (Fig. 1c-f) and tight junctions (Fig. 1c-e). Microvilli (Fig. 1d and g) are also evident on the apical side. Exposure to air may be required for cilia development. Extracellular matrix simulating the basement membrane is also present (Fig. 1f).

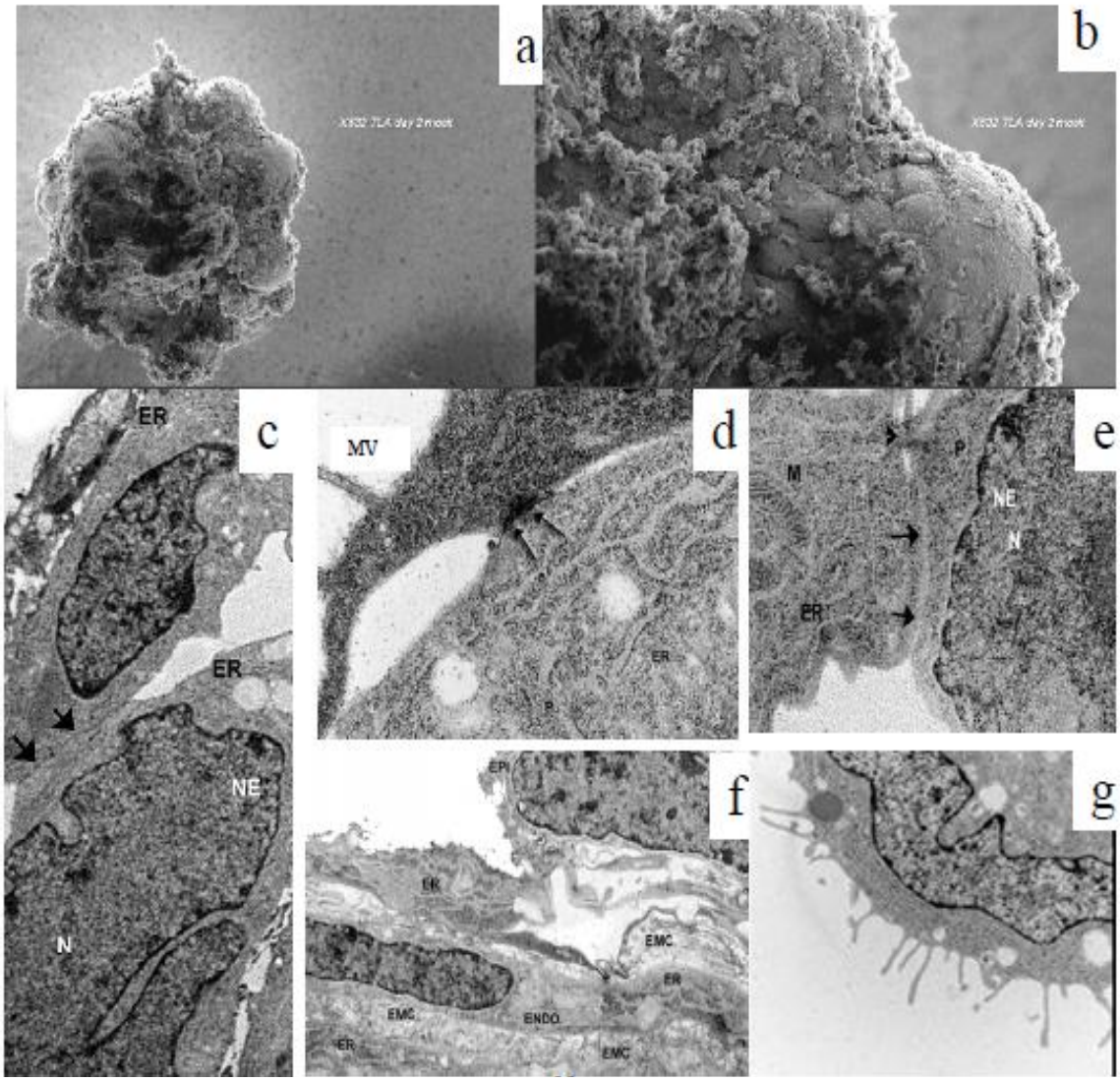

Figure 1. 3D HBE TLAs have characteristics of the human respiratory epithelium. 3D HBE TLAs grown on Cytodex 3 beads in modeled microgravity for 31 to 35 days as depicted by scanning electron microscopy (a and b) (magnification: 286x and 1100x, respectively). Transmission electron microscopy of sections of 3D HBE TLAs grown in modeled microgravity for 31 to 35 days (c-f) showing multiple cell types (as indicated by the morphology of cells and nuclei), multiple layers of cells (c-f), extracellular matrix (f), microvilli (d, g), polarization (d, g), tight junctions (arrows) (c-e), and hemidesmosome (arrowhead) (e). Endothelial cells are longer than wide, with long narrow nuclei and no microvilli. Epithelial cells are robust with compact nuclei and microvilli. EMC = extracellular matrix, ENDO = endothelial cell, EPI = epithelial cell, ER = endoplasmic reticulum, M = mitochondria, MV = microvilli, N = nucleus, NE = nuclear envelope, P = polyribosomes. Original magnifications are 5000x (c), 25,000x (d), 10,000x (e), 7500x (f), and 12,000x (g).

Expression of HRE-specific markers

Fixed TLAs, HBTC monolayers, BEAS-2B monolayers, and normal human lung were immunostained for epithelial-specific cell markers to evaluate the cellular composition and differentiation state (Fig. 2). The markers were selected to highlight epithelial characteristics including tight junctions (ZO-1), and polarization (epithelial membrane antigen [EMA]). Expression of ICAM-1 and cytokeratin 18 highlight a differentiated state. Expression of mucin glycoprotein indicates the potential to produce mucus. As illustrated, expression levels of epithelial markers in TLAs are very similar to the levels in normal human lung than in 2D BEAS-2B and HBTC cells. Note that the staining of ZO-1 is concentrated at cell junctions in 3D HBE TLAs as in the human lung. There may be low expression of ZO-1 in HBTC monolayers, but the staining is more diffuse. A neuronal-specific marker, microtubule associated protein 2 (MAP2), is not expressed in 3D HBE TLAs but is expressed in 3D normal human neural progenitor cells.

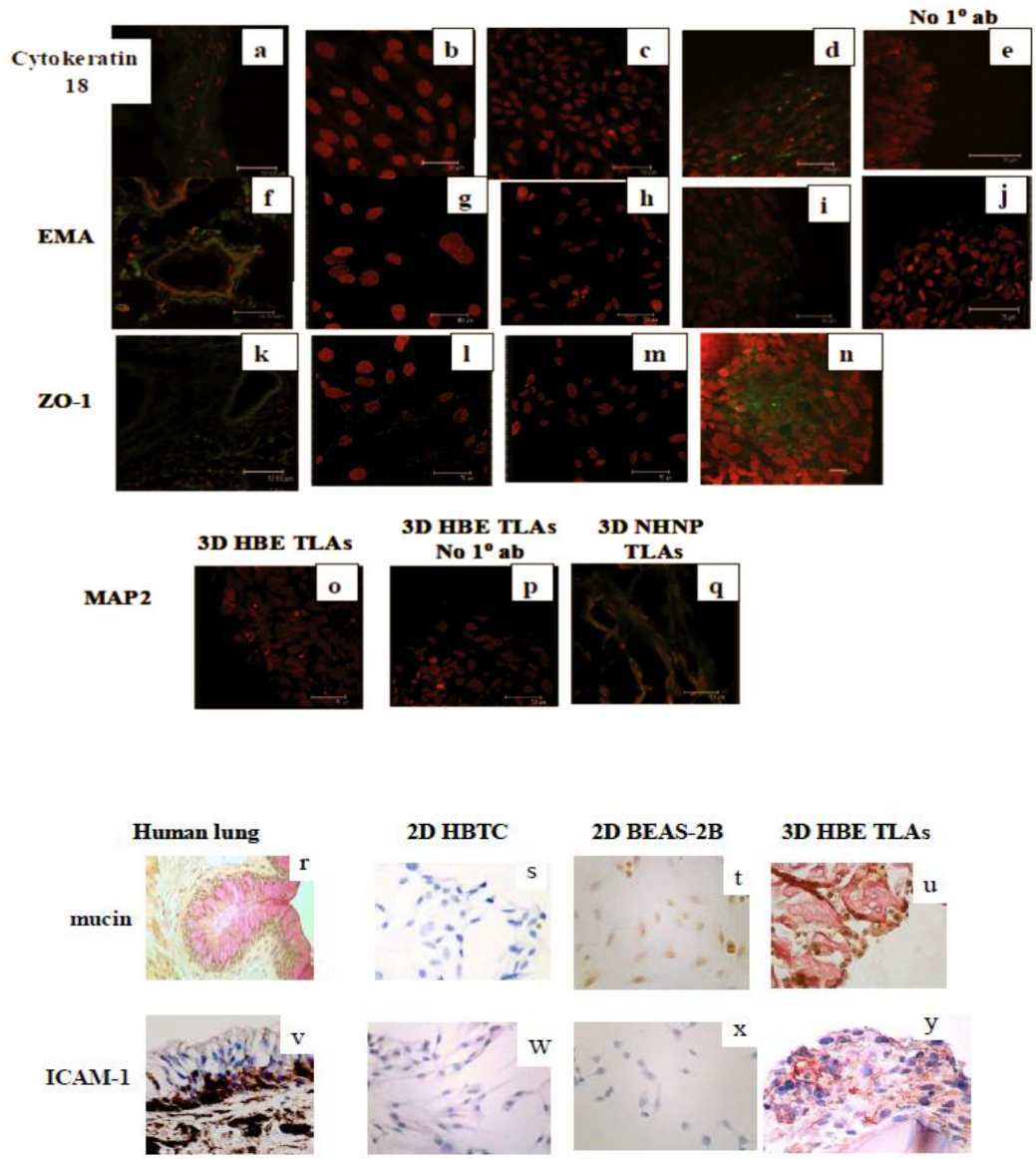

Figure 2. 3D HBE TLAs express markers of the human respiratory epithelium. Cells in panels a-q were immunostained with fluorescent primary or secondary antibodies and analyzed by confocal microscopy. Cell nuclei are red and the epithelial markers are green. Antibody to one neuronal marker antibody was used to illustrate specificity (green). Panels a, f, k, r, and v are human lung sections; panels b, g, l, s, and w are HBTC monolayers; panels c, h, m, t, and x are BEAS-2B monolayers; panels d, I, n, o, u, and y are 3D HBE TLAs; and panels e, j, p, are 3D HBE TLAs without the primary antibody. Panel q is 3D NHNP cells. A 1:25 dilution of the cytokeratin 18 antibody was used to stain the cells in panels a-e; a 1:1500 dilution of the EMA antibody was used to stain the cells in panels f-i; a 1:5000 dilution of the ZO-1 antibody was used to stain the tight junctions in panels (k-n) (ZO-1 ab was already conjugated to Fluorescein isothiocyanate so a control lacking this primary antibody was not performed); and a 1:40 dilution of the antibody for a neuronal specific marker, MAP2 was used to stain cells in panels o-q. Magnification bars are shown on each photograph a-q. Antibodies to mucin were used to stain r-u by immunhistochemistry (pink); and an antibody to ICAM-1 was used to stain v-y by immunhistochemistry (light to dark brown). Original magnifications were 400X.

Gene expression in BEAS-2B monolayers and 3D HBE TLAs

Cellular differentiation involves complex cellular interactions.[22] Not only do cell membrane junctions, extracellular matrices, and soluble autocrine and paracrine factors [23-26] play a significant role in tissue development, but also the spatial orientation and spatial relationships of the layered cells. The fact that each HBE cell has three membrane surfaces, a free apical surface, a lateral surface, and a basal surface[19] that interacts with mesenchymal cells enhances differentiation and cell-to-cell communication in epithelial cells grown in modeled microgravity compared to traditional monolayers. An important role of the HRE is to produce an innate immune response to pathogens in the airway. Transcriptional profiling results (Fig. 3) also indicate a higher number of genes involved in immune response, immunological and inflammatory diseases are upregulated in uninfected 3D HBE TLAs as compared to BEAS-2B monolayers. Most importantly, the profile of cytokines secreted from uninfected TLAs (Fig. 9a) parallel the profile detected in human airways as described elsewhere.[17]

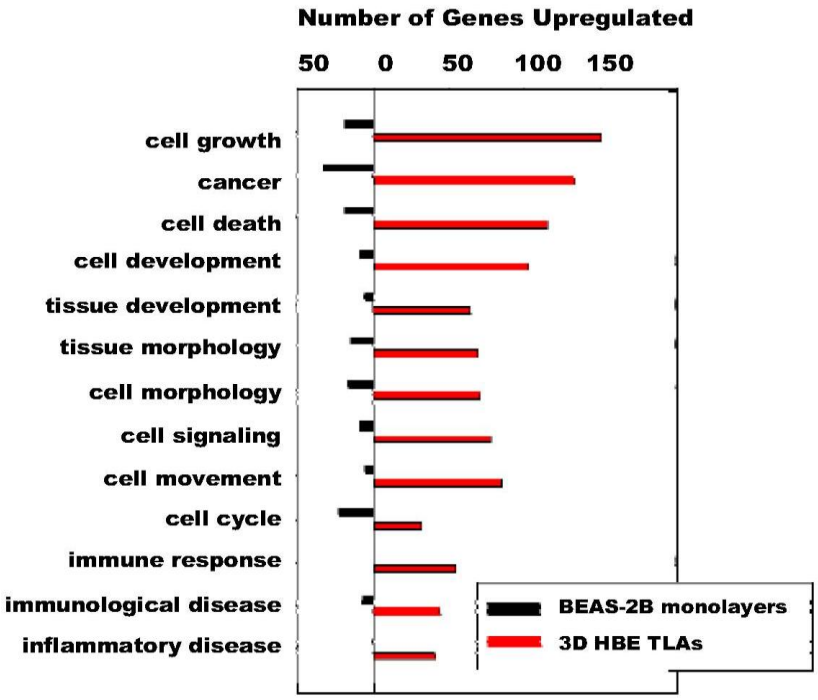

Figure 3. Higher levels of cell development, cell signaling, and cell growth as well as immune response are expressed in 3D HBE TLAs compared to BEAS-2B monolayers.

wtRSV and wtPIV3 replicate more efficiently than mutants in TLAs

To compare the replication efficiencies of different RSV and PIV3 strains grown in different culture conditions, monolayers and TLAs were infected at 35°C—the upper temperature of the upper HRE. Culture samples were collected on different times post infection (pi) to quantify the virus. Peak replication of *wt*RSVA2 and attenuated strains *cpts*248/404 and rA2cpΔNS2, were similar in Vero and BEAS-2B epithelial cell monolayers (Fig. 4a and b). The 2 $\log_{10}$ pfu/mL reduction in titer of *wt*RSVA2 from day 2 to 7 in Vero cells (Fig. 4a) resulted from destruction of the monolayer. In contrast in HBE TLAs, attenuated strains, *cpts*248/404 and rA2cpΔNS2 replicated to a peak titer of 3-4 $\log_{10}$ pfu/mL, significantly lower than the peak titer of 6 $\log_{10}$ pfu/mL of *wt*RSVA2 (Fig. 4c). Hence, a significant difference in replication of *wt*RSV and attenuated viruses was clearly differentiated in TLA cultures as *in vivo.*[12, 14] The fact that innate immunity pathways are more highly expressed in HBE TLAs than monolayers (Fig. 3) may play a role in attenuation. *wt*PIV3 (JS), Bovine PIV3 Shipping Fever virus (bPIV3 SF), and PIV3-cp45 each replicated to $\geq$ 8 $\log_{10}$ pfu/mL by day 4 pi in 2D monkey kidney LLC-MK2 cells. Lower replication efficiency observed for PIV3-cp45 only on day 6 and 8. Host restriction of bPIV3 SF, however, was not observed in LLC-MK2 cells (Fig. 4d). In epithelial BEAS-2B monolayers, PIV3-cp45 replicated 1.5 to 2 $\log_{10}$ pfu/mL lower than *wt*PIV3 JS from day 4 to 8, suggesting an attenuated phenotype in this cell line; however, the replication levels of *wt*PIV3 JS and bPIV3 SF were similar (Fig. 4e). In HBE TLAs, replication of JS approached 7.5 $\log_{10}$ pfu/mL by day 6 pi, while PIV3-cp45 and bPIV3 SF replicated maximally to 5.5 and 3.5 $\log_{10}$ pfu/mL on day 6, respectively, and to 6 $\log_{10}$ pfu/mL by day 10 (Fig. 4f). Similar to RSV strains, the attenuated PIV3 viruses replicated less efficiently than *wt*PIV3 in HBE TLAs. Growth restriction of the attenuated strains may be due to a slower progression from layer to layer in 3D HBE TLAs. More detached cells were observed in infections with wild type viruses than infections with the attenuated strains.

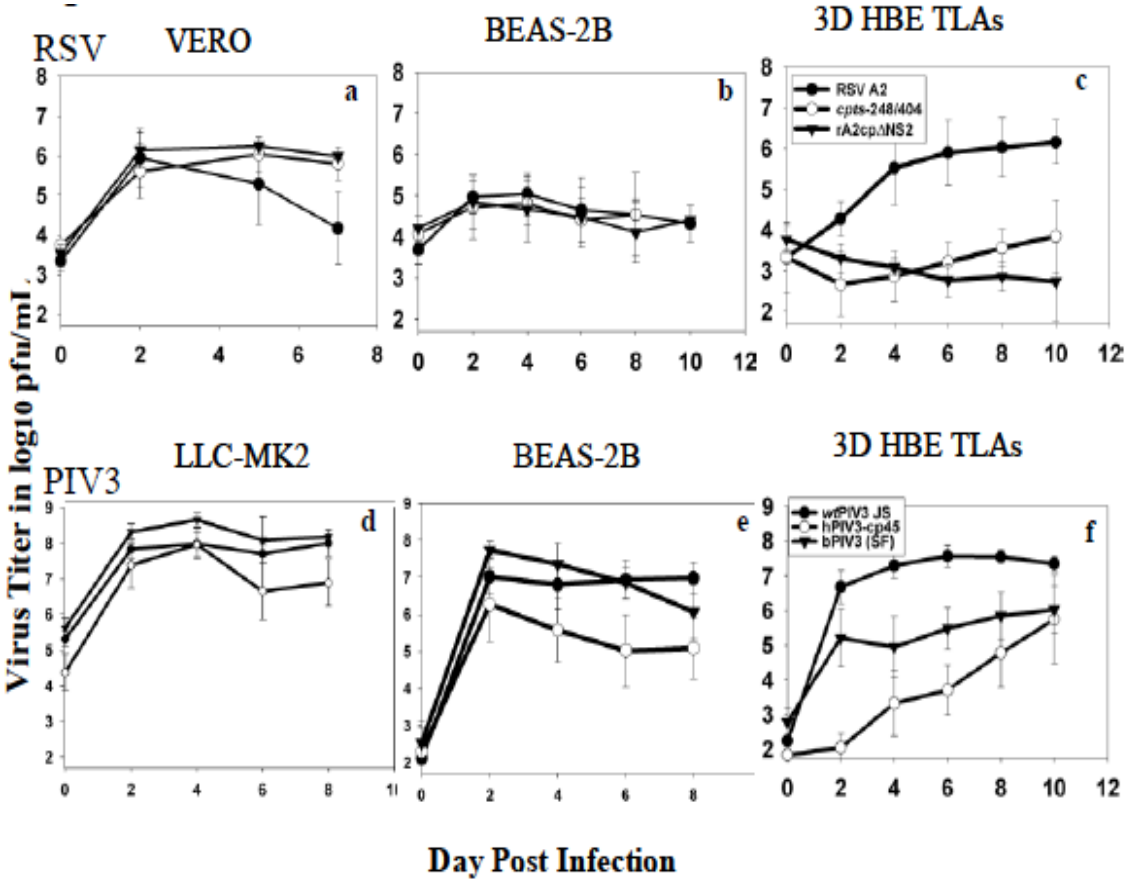

Figure 4. Replication efficiencies of *wt*RSVA2 and *wt*PIV3 JS are significantly higher than attenuated strains in 3D HBE TLAs. Samples were collected on days 0, 2, 5, and 7 for Vero, days 0, 2, 4, 6, and 8 for LLC-MK2; days 0, 2, 4, 6, and 8 RSV-infected BEAS-2B, days 0, 2, 4, 6, 8, and 10 for PIV3-infected BEAS-2B; and days 0, 2, 4, 6, 8, and 10 (pi) for TLAs. The geometric mean virus titers from three experiments for Vero and LLC-MK2 infections and six to eight experiments in 2D and 3D epithelial cells were calculated and plotted against time after infection in 2D Vero cells (a), 2D BEAS-2B (b and e), 2D LLC-MK2 (d), and 3D HBE TLAs (c and f). The error bars represent the standard deviations. Virus only (no cells) control is also shown in panel c.

Innate immune response to RSV and PIV3 infection

Table I lists the cytokines, chemokines, and colony-stimulating factors detected in cell culture supernatants from wild type infected BEAS-2B epithelial cells and 3D HBE TLAs in comparison to a limited number of nasal washes from *wt*PIV3-infected children. For infected samples, only those cytokines with mean secretion levels $\geq$ twofold higher than uninfected samples are listed. Of the 19 tested, most of the epithelial-derived cytokines induced by *wt*PIV3-infected children were also secreted by infected TLAs, except TNF-α. Of the 19 tested, most of the epithelial-derived cytokines induced by RSV-infected patients[27] were also secreted by

infected HBE TLAs, except MCP-1 and TNF-α. It is likely non-epithelial cells contribute to the higher levels of TNF- α and MCP-1 in the airways of infected patients. *Wt*RSV-infected-2D BEAS-2B cells secreted ≥ twofold increases (relative to uninfected) of IL-6, IL-8, RANTES, MIP-1α, MIP-1–, MCP-1, and IFN-γ but not IL-1–, GM-CSF, and G-CSF as in infected TLAs. *wt*PIV3-infected BEAS-2B cells secreted ≥ twofold increases (relative to uninfected) of IL-6, IL-8, RANTES, and IFN-γ but not MIP-1α, MIP-1–, IL-1–, GM-CSF, and G-CSF and IL-4 as in HBE TLAs.

Table I

Sample[b]	**Secreted Cytokines, Chemokines, and Colony Stimulating Factors**[a]			
	***wt*RSV-infected**[c]		***wt*PIV3-infected**[c]	
2D BEAS-2B[c,d]	IL-6 IL-8 RANTES MIP-1α	MIP-1– MCP-1 INF-γ	IL-6 IL-8 RANTES IFN γ	
3D HBE TLAs[c,d]	IL-6 IL-8 RANTES MIP-1 α MIP-1–	IL-1– GM-CSF G-CSF	IL-6 IL-8 RANTES MIP-1 α MIP-1–	IL-1– GM-CSF G-CSF IL-4
Human Nasal Wash	ND		IL-8 RANTES MIP-1 α MIP-1–	IL-1– G-CSF TNF-α

[a] A total of 17 were tested using the BioPlex Human Cytokine Assay kit (BioRad) and 3 were tested by ELISA (RANTES, MIP-1α, and INF-–)

[b] Approximately tenfold more cells were present in 3D HBE TLAs than BEAS-2B monolayers. Epithelial cell numbers were not determined for the human nasal wash samples.

[c] The mean secretion levels of the cytokines listed were > twofold higher than corresponding mock-infected samples or nasal washes from healthy subjects.

[d] day 2 and/or day 8 pi

ND= not done

TLAs predict in vivo inflammatory responses

Figure 5a illustrates the average fold increases of secreted levels of cytokines from a limited number of nasal washes collected from children infected with *wt*PIV3 or vaccinated with PIV3-cp45 relative to levels from normal healthy controls. The difference in levels of secreted IL-1–, IL-8, MIP-1α, MIP-1–, RANTES, and G-CSF between *wt*PIV3 and healthy controls are statistically significant (Table II). The difference in the levels of IL-1–, IL-8, MIP-1 α, and

RANTES in nasal washes from *wt*PIV3- and PIV3-cp45-infected children are also statistically significant. Importantly, the differences in cytokine levels were not significant between the PIV3-cp45 and control nasal washes. The mean fold increases of cytokines secreted from wild type and attenuated PIV3- and RSV-infected TLAs from day 0 to 2 pi and 6 to 8 pi are illustrated in Fig. 5b and c. Similar to the cytokines present in the human nasal washes, the levels of the cytokines secreted from HBE TLAs were higher than the levels secreted from TLAs infected with bPIV3 and PIV3-cp45 and statistically significant in the day 6 to 8 samples (Table II). Similar results are illustrated for TLAs infected with *wt*RSVA2 relative to TLAs infected with *cpts*248/404 and rA2cpΔNS2. Similar to the nasal wash levels of IL-8, MIP-1α, and RANTES, potential biomarkers of inflammation, the differences in levels secreted from TLAs infected with wild type and attenuated strains are statistically significant (Table II).

Table II. Statistical Significance of Cytokine Levels in Nasal Washes, 3D HBE TLAs, and 2D BEAS-2B Cells

Nasal Wash Samples	**IL-1β**	**IL-6**	**IL-8**	**MIP-1α**	**MIP-1β**	**RANTES**	**G-CSF**	**GM-CSF**
wt PIV3 vs. PIV3 neg	0.03	0.051	0.018	0.014	0.035	0.027	0.049	inc
wt PIV3 vs. PIV3-cp45	0.03	0.08	0.022	0.045	0.105	0.002	0.089	inc
PIV3-cp45 vs. PIV3 neg	1.000	1.000	0.941	0.58	0.592	0.205	0.771	inc
3D HBE TLA Samples*	**IL-1β**	**IL-6**	**IL-8**	**MIP-1α**	**MIP-1β**	**RANTES**	**G-CSF**	**GM-CSF**
wt PIV3 vs. mock	<.0001	0.0063	0.0009	0.0349	0.0002	<.0001	0.0009	<.0001
wt PIV3 vs. PIV3-cp45	0.0001	0.0558	0.074	0.0478	0.0056	0.002	0.0036	0.0024
PIV3-cp45 vs. mock	0.129	0.292	0.0396	0.708	0.1024	0.031	0.3845	0.0579
2D BEAS-2B Samples*	**IL-1β**	**IL-6**	**IL-8**	**MIP-1α**	**MIP-1β**	**RANTES**	**G-CSF**	**GM-CSF**
wt PIV3 vs. mock	0.0264	<.0001	0.0004	0.8603	0.098	0.2627	0.2487	0.2371
wt PIV3 vs. PIV3-cp45	0.0454	0.0067	0.1122	0.334	0.3561	0.6652	0.2487	0.9464
PIV3-cp45 vs. mock	0.758	0.0001	0.0059	0.2681	0.4114	0.4757	1.0000	0.262

mock = mock infected or uninfected
inc = inconclusive
* day 8 samples

In contrast, the cytokine secretion levels were sometimes higher in 2D BEAS-2B cells infected with attenuated viruses than wild type virus (Fig. 5d and e); i.e., MIP-1α and RANTES in bPIV3 SF and rA2cpΔNS2 infections. Lower fold increases of these chemokines from wild type infected cells may be explained by cytopathic effect of day 8 but not day 2 monolayers. The fold increases of RANTES secretion levels were extremely high in day 2 RSV-infected BEAS-2B cells and, thus, graphed separately (inset).

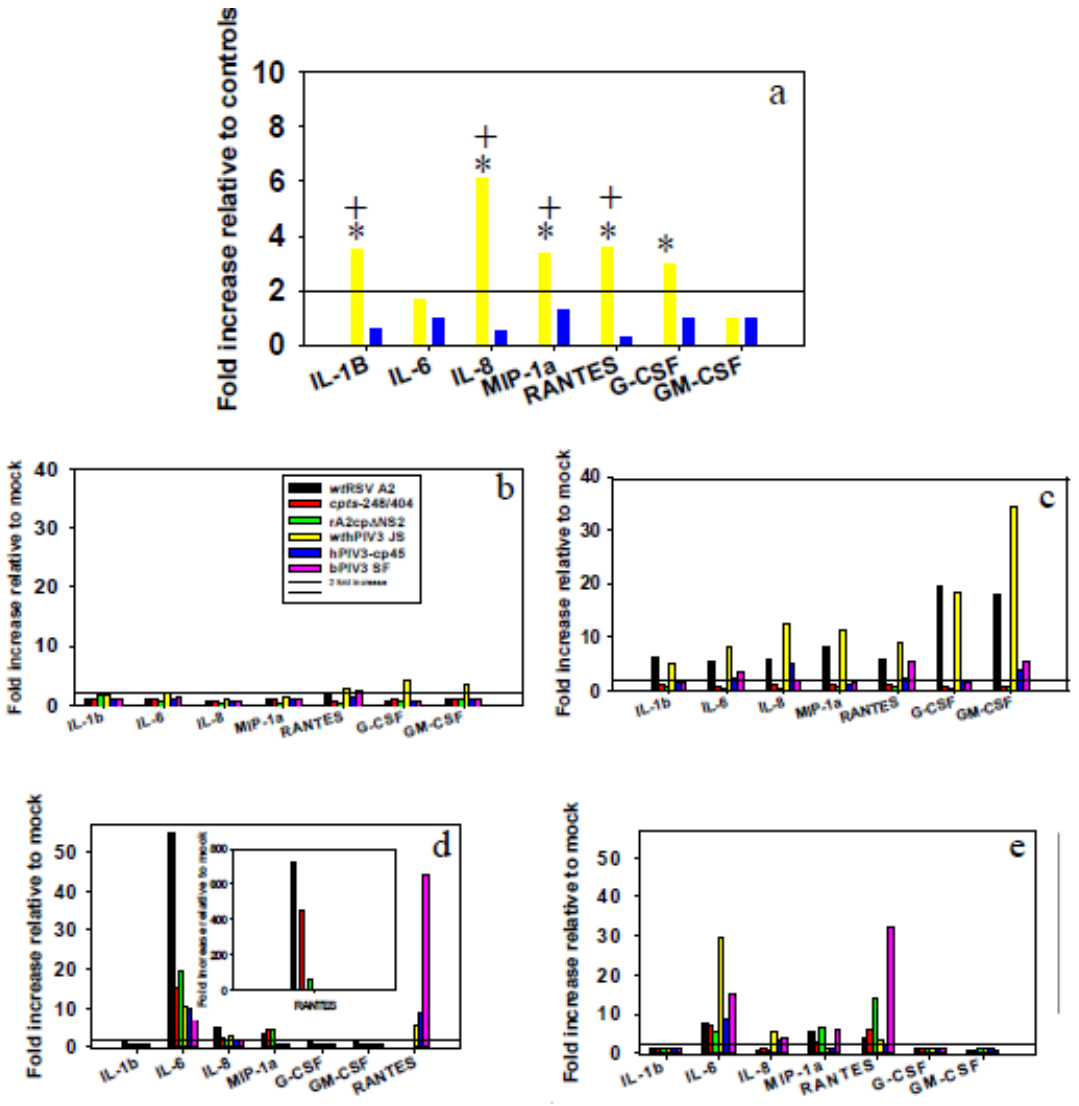

Figure 5. **Fold increases of representative cytokines secreted from wild type infected 3D HBE TLAs are significantly higher than secreted levels from infections with attenuated strains.** (a) Fold increases of cytokines (IL-1–, IL-6), chemokines (IL-8, MIP-1α, RANTES) and colony-stimulating factors (G-CSF, GM-CSF) in nasal wash samples collected from subjects shedding *wt*PIV3 and attenuated PIV3-cp45 were calculated relative to normal healthy controls. Statistically significant differences in levels between nasal washes collected from subjects shedding *wt*PIV3 and normal healthy controls is indicated (*); statistically significant differences in cytokine levels between nasal washes collected from subjects shedding *wt*PIV3 and PIV3-cp45 is indicated(+). Cytokines (IL-1–, IL-6), chemokines (IL-8, MIP-1α, RANTES), and colony-stimulating factor (G-CSF, GM-CSF) after infection with wild type and attenuated RSV and PIV3 virus strains were plotted as fold increases relative to corresponding mock-infected cells or uninfected cells that were treated similarly to infected cells without the virus; (b) Day 0-2 3D HBE TLAs (day 0 represents collection of a sample just after virus adsorption); (c) Day 6-8 3D HBE TLAs; (d) Day 0-2 2D BEAS-2B cells; (e) Day 6-8 2D BEAS-2B cells. A line was added to emphasize a twofold increase relative to mock. The fold increase in RANTES for RSV-infected cultures is presented in inset (d) because of the different scales. One experiment was performed with human nasal washes and a total of 6-8 experiments were performed in 2D BEAS-2B and 3D TLAs. The mean secretion levels were determined in JMP software.

Low secretion levels of cytokines from TLAs infected from days 0 to 2 (Fig. 5b) relative to days 6 to 8 (Fig. 5c) suggest an association with virus titer (Fig. 4c and 4f). Therefore, the Spearman's correlation value between the cytokine secretion levels and virus titer was determined by plotting the log of the cytokine/chemokine concentration against the titer (in $\log_{10}$ pfu/mL) of *wt*RSV A2 and *wt*PIV3 JS on day 0, 2, and 8 pi (Fig. 6 and Table 3). As illustrated, the correlation is higher in HBE TLAs than BEAS-2B monolayers for all secreted pro-inflammatory mediators tested IL-1−, IL-6, MIP-1α, RANTES, G-CSF, and GM-CSF, except for IL-8 in *wt*RSV A2 infected cultures. All the Spearman correlation values for 3D HBE TLA infections were statistically significant. The Spearman correlation values are generally higher for *wt*PIV3 JS infected-HBE TLAs than *wt*RSV A2 most likely because of its higher replication efficiency. The correlation of IL-6, IL-8, and RANTES secreted from *wt*RSV A2 infected-BEAS-2B cells and IL-6 and IL-8 from wtPIV3 JS infected-BEAS-2B cells and virus titer was statistically significant.

Table III

Cytokines	wtRSVA2				wtPIV3 JS			
	BEAS-2B		3D HBE TLAs		BEAS-2B		3D HBE TLAs	
	Spearman value	p value	Spearman value	p value	Spearman value	p value	Spearman value	p value
IL-1B	0.4686	0.498	0.7142	<.0001	0.0493	0.8459	0.9057	<.0001
IL-6	0.6496	0.0035	0.6606	<.0002	0.5611	0.0154	0.8029	<.0001
IL-8	0.7505	0.0003	0.6146	0.0011	0.5474	0.0187	0.8642	<.0001
MIP-1a	0.6441	0.0612	0.7738	<.0001	-0.55	0.125	0.8519	0.0001
RANTES	0.6794	0.0019	0.8432	<.0001	-0.0994	0.7401	0.8281	<.0001
G-CSF	0.3506	0.1507	0.747	<.0001	-0.0234	0.9265	0.8195	<.0001
GM-CSF	0.3506	0.1537	0.7932	<.0001	-0.0234	0.9265	0.8898	<.0001

Spearman correlation value is the nonparametric r value for the linear correlation between the log concentration of the cytokine and virus titer in $\log_{10}$ pfu/mL.
p value indicates statistical significance if <0.05.

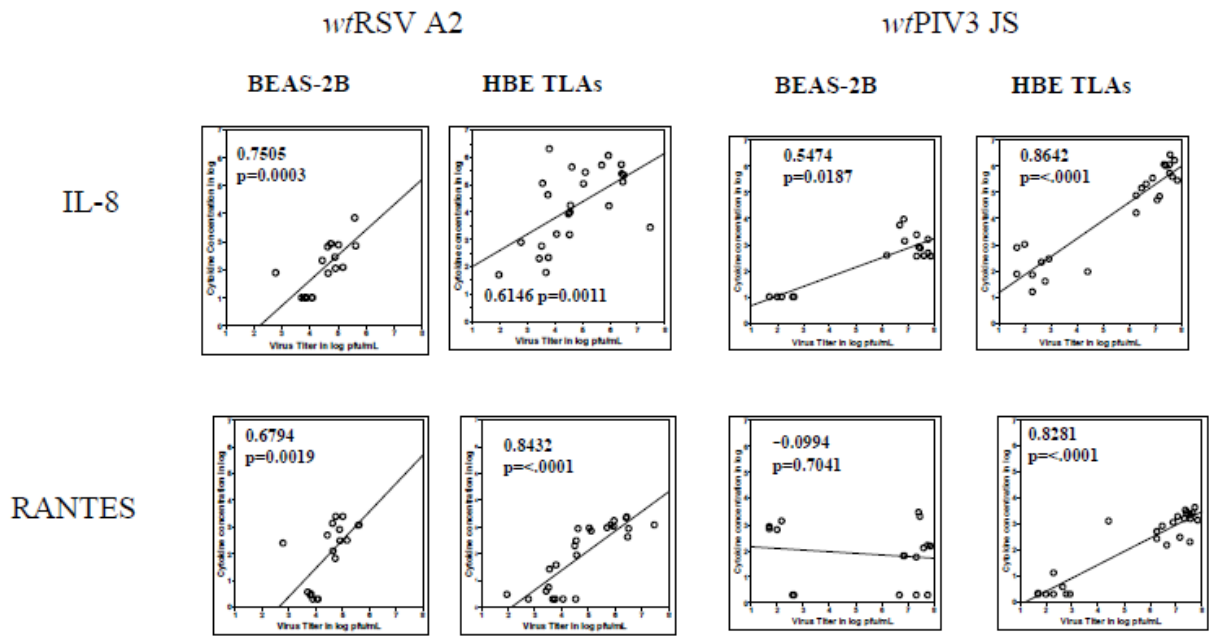

Figure 6. Correlation of levels of cytokines, chemokines, and colony-stimulating factors with virus titer. The log concentration of cytokines on day 0, 2, and 8 for *wt*RSV A2 and *wt*PIV3 JS infections in 2D BEAS-2B cells and 3D HBE TLAs were plotted against the virus titer in log pfu/mL on the same days pi using the JMP statistical program. The Spearman correlation value (determined in JMP) is illustrated on each graph and in Table III. Illustrated here are the graphs of two examples, IL-8 and RANTES. P = p value, <0.05 is statistically significant.

2.0 Discussion

Lacking large-scale *in vitro* cell culture models and small animals that mimic human respiratory virus infections and disease states has hindered the development of live attenuated RSV and PIV3 vaccines. For example, although 4.2 $\log_{10}$ pfu/mL of *cpts*248/404 was shed on average into the nasal cavities of 3- to 5-month-old infants receiving 10^5 pfu,[12] only 2.2 $\log_{10}$ pfu/mL[28] and 1.3 $\log_{10}$ pfu/mL[29] was shed by in mice and chimpanzees, respectively, after receiving 10^6 pfu. 4.3 $\log_{10}$ pfu/mL of rRSVA2248/404ΔSH was shed on average into the nasal cavities of seronegative children with a 10^5 pfu[30] and only 2.1 $\log_{10}$ pfu/mL in chimpanzees with a 10^5 pfu.[31] 4.3 $\log_{10}$ pfu/mL of rRSVA2248/404/1030 was shed on average into nasal cavities of seronegative children after a 10^5 pfu dose[30] and no rRSVA2248/404/1030 was detected in nasal turbinates of mice after a 10^6 dose.[28] Therefore, we engineered a novel *in vitro* model of the HRE to predict *in vivo* attenuation levels of cp, *ts*, host-range (hr), and gene deleted viruses. As reported here, growth of two respiratory viruses in 3D HBE TLAs and the

concomitant host response parallel infections of the HRE more closely than 2D epithelial cells.

Differences in structural organization and state of differentiation affect the physiology of epithelial cells[32] grown as monolayers or TLAs. As in the HRE, the multiple cell types in the TLAs are organized in layers. Intrinsic to the higher complexity of TLAs and different membrane interactions is a cascade of events essential not only to architecture but also to differentiation.[19] Therefore, TLAs display hallmarks of *in vivo* epithelia, express markers of differentiated epithelial cells, and induce cell growth, and cell signaling pathways not present in 2D cells. Cell communication through intercellular junctions, paracrine factors, and cell adhesion molecules are important to epithelial function.[20] Thus, TLAs represent a more physiologically relevant model of the HRE than 2D epithelial cells. One difference is that TLAs produce microvilli instead of the cilia of the HRE. Since cilia play an important role in virus infection,[33] this difference between the HBE TLAs and HRE may not be significant since virus infections in HBE TLAs parallel *in vivo* RSV infections (Deatly et al, submitted).

This novel 3D HBE TLA model has some significant advantages with respect to existing *in vitro* cultures of the HRE, such as primary cell and air liquid interface cultures. The capability for large-scale production and prolonged culture and infection times provide the ability to remove aliquots for multiple analyses at different times pi without terminating the experiment, thus eliminating the cost and uncertainly of restarts. The ease of maintaining consistent cultures allows comparison of data from experiments of different batches of HBE TLAs. Our polarized multicellular HBE TLA model of cells from the human bronchi and tracheae better mimics the upper respiratory tract than the 3D monoculture of alveolar A549 epithelial cells.[34]

A hallmark of RSV and PIV3 infection in traditional monolayer cultures is the formation of syncytial or large multinucleated cells resulting from cell fusion. Syncytia are not always detected in the respiratory tract of fatal RSV cases[35] and have not been observed by Transmission Electron Microscopy of HBE TLA tissue sections or in the air liquid interface culture infections.[33] In polarized epithelia, expression of the fusion protein is restricted to the apical surface; therefore, it is not able to interact with adjacent cells. Syncytia formation may be more prevalent in infections of monolayers or thin epithelial layers *in vivo*. Therefore, we hypothesize paramyxovirus infections in HBE TLAs may mimic *in vivo* infections more closely than infections in traditional monolayers.

Small Phase I clinical trials are performed to evaluate the safety and immunogenicity of vaccine candidates. Three criteria of safety include attenuation, phenotypic/genetic stability,

and clinical symptoms of respiratory disease. In clinical trials, *cpts*248/404 and PIV3-cp45 were attenuated and stable when 10^5 pfu were administered to children and infants.[12,13] rA2cpΔNS2 was over-attenuated in adults when intranasally administered even at 10^7 particle-forming units.[14] The bPIV3 SF is attenuated in rhesus macaques[15] and most likely hr restricted in humans as the bPIV3 Kansas strain.[36] Like *in vivo*, attenuated RSV and PIV3 strains produce significantly lower titers than respective wild type viruses in TLAs at 35°C—the upper temperature of the upper HBE.[11] Although attenuated RSV strains *cpts*248/404 and rA2cpΔNS2 replicated at lower titers (0.5 and 0.9 $\log_{10}$ pfu/mL, respectively) than *wt*RSVA2 in primary submerged human adenoid epithelial cells at 35°C,[37] virus titers of these strains were 2 to 3 $\log_{10}$ pfu/mL lower in HBE TLAs. Most likely improved cell communication and cell signaling in TLAs facilitate the differentiation of replication levels of wild type and attenuated viruses not observed in 2D cells or air liquid interface cultures.

A fundamental role of the HRE is to prevent microbial invasion. Pro-inflammatory mediators *in vivo*[17] recruit inflammatory cells that clear the virus by phagocytosis. Similarities in the profiles of pro-inflammatory mediators between epithelial cells *in vitro* and *in vivo* indicate that epithelial cells are likely the primary secretors of these mediators even prior to microbial invasion.

Although disease pathogenesis is generally associated with replication efficiency and cytotoxicity of the pathogen, severe disease states resulting from RSV (and most likely PIV3) are due to the inflammatory response to the virus.[38] As illustrated in Fig. 7, the innate immune response of the HRE to RSV results in secretion of cytokines (IL-1, TNF-α, IL-6, and IL-11), and chemokines (IL-8, MIP-1α, RANTES, and MCP−1)[27,38-42] (Fig. 7b). These pro-inflammatory mediators elicit inflammatory cells.[43] In mild disease states, inflammatory cells, primarily neutrophils, eosinophils, and macrophages, phagocytose virus to clear the airway and as part of the process produce an antiviral response (Fig. 7c). Severe disease states are characterized by airways constricted with inflammatory cells (Fig. 7d), shed epithelial cells, and mucus accumulation.

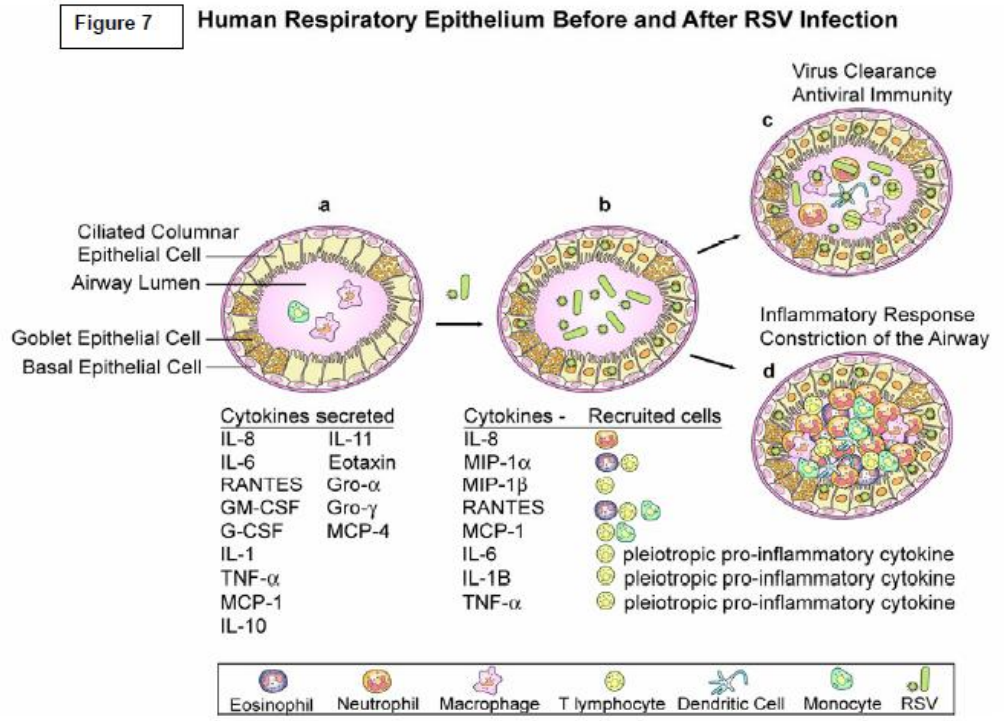

Figure 7. **A diagram of the stages of RSV-infected HRE** (a) before RSV infection (cytokines in the first column were tested in our assays); (b) RSV infection and the cytokines and chemokines induced in response to infection and the inflammatory cells they recruit[43]; (c) a mild disease state in which the inflammatory cells clear RSV from the airway by phagocytosis; (d) a severe disease state in which the inflammatory cells constrict the airways.

Elevated levels of MIP-1α, MCP-1, RANTES, and IL-8 are associated with human RSV disease and may correlate with disease severity.[44-50] IL-8 is the most potent chemoattractant for neutrophils and comprises up to 93% of the cells in the airway lumen in bronchiolitis cases. RANTES and MIP-1α, potent chemoattractants of eosinophils comprising up to 8% of the cells in the airway, are associated with bronchospasms.[38,51] Higher levels of these pro-inflammatory chemokines may elicit higher numbers of inflammatory cells, thus increasing the likelihood for constriction of the airways, especially in infants.[52] In this case, elevated levels of IL-8, MIP-1α, MCP-1, and RANTES may serve as biomarkers for clinical inflammation. In the current study, *wt*RSV and *wt*PIV3 induce statistically higher secretion levels of pro-inflammatory mediators than attenuated strains in TLAs from day 6 to 8, paralleling the results from nasal washes collected from subjects with *wt*PIV3 infections and vaccinees that received PIV3-cp45 intranasally. Furthermore, the low levels of pro-inflammatory mediators in nasal washes from PIV3-cp45 vaccinees and healthy controls were not statistically different, correlating with a lack

of clinical symptoms of inflammation of the vaccines.[12,13] Therefore, low cytokine secretion levels from *cpts*248/404 and rA2cpΔNS2-infected TLAs are also consistent with clinical observations in Phase I studies since these vaccinees also lacked symptoms of inflammation.[12,14] Especially noteworthy are the significant differences in secretion levels of IL-8, MIP-1α, and RANTES between wild type and attenuated strains in nasal washes since their levels were associated with severity of RSV disease in humans. Statistically significant differences between the cytokine levels in infected and uninfected TLAs are more similar to infected and uninfected nasal washes than 2D BEAS-2B cells. One difference is the secretion of GM-CSF from TLAs that is not detected in nasal washes collected from *wt*PIV3-infected subjects. Since epithelial or mesenchymal cells secrete GM-CSF, perhaps a factor not expressed in the TLAs inhibits induction of GM-CSF in the HRE.

Since attenuation level and low secretion levels of pro-inflammatory cytokines of *cpts*248/404, rA2cpΔNS2, and PIV3-cp45 in TLAs correlate with safety in clinical trials, the low replication efficiency and low secretion levels of pro-inflammatory mediators of bPIV3 SF in TLAs predict that this strain would also be safe in humans. Indeed a similar strain, bPIV3 (Kansas), was safe in humans.[36] In contrast, similar replication efficiency and higher secretion levels of MIP-1α and RANTES in infected BEAS-2B monolayers relative to *wt*PIV3 infections would suggest that bPIV3 SF and rA2cpΔNS2 would not be safe in humans.

In summary, the parallels between cell physiology, viral growth kinetics, and pro-inflammatory mediator profiles substantiate the physiological relevance of TLAs to human respiratory epithelia compared to 2D BEAS-2B cells. The 3D HBE TLA model offers an advantage over monolayer cultures in predicting the level of attenuation and the inflammatory response of respiratory viruses in humans. Therefore, RSV and PIV3 infections in HBE TLAs may mimic *in vivo* infections more closely than infections in traditional monolayers. The data indicate HBE TLAs may be better suited to evaluate RSV and PIV3 vaccine candidates prior to clinical trials.

3.0 Methods

Cells

Mesenchymal cells (HBTC) from human bronchi and tracheae were obtained from three donors through Cambrex Biosciences (Walkersville, MD). LLC-MK2 and BEAS-2B epithelial cells[53] were obtained from ATCC (Manassas, VA). BEAS-2B cells were used instead of primary cells to provide consistency from batch to batch. BEAS-2B and HBTC cells were maintained in GTSF-2 medium with 7% fetal bovine serum[9] in human fibronectin coated flasks (BD Biosciences, San Jose, CA). Vero, HEp-2, and LLC-MK2 cells were grown at 37°C in Eagle's modified minimum essential medium supplemented with 2mM non-essential amino acids, 100 units penicillin, 100 µg/ml streptomycin, 0.25 µg/ml amphotericin B, 10% fetal bovine serum, 2mM L-glutamine, and 25mM HEPES buffer (Gibco-BRL, Gaithersburg, MD).

3D TLA cultures

To construct 3D HBE TLA cultures, HBTC cells from a monolayer culture were seeded at 2 x 10^5 cells/mL into a 55-mL rotating wall vessel (RWV) (Synthecon, Houston, TX) with 4-5 mg/mL of Cytodex-3 microcarriers, type I collagen-coated cyclodextran microcarriers (Pharmacia, Piscataway, NJ) at 35°C. Cultures were allowed to grow for a minimum of 48 hours before the medium was changed. BEAS-2B cells were seeded at 2 x 10^5 cells/mL 4 to 6 days after HBTC-Cytodex 3 microcarrier aggregates were formed. Thereafter, approximately 65% of the media was replaced every 20 to 24 hours. As metabolic requirements increased, the glucose concentration in GTSF-2 medium was increased to 200 mg/dL. TLA cultures were grown in RWV to 1 to 2 mm in diameter using the rotary cell culture system (Synthecon, Houston, TX) at 35°C with appropriate rotation rate for aggregate suspension. Cell numbers were determined after treating the TLAs with 2000U/mL type I collagenase (Invitrogen, Carlsbad, CA) at 37°C for 10 minutes.

Viruses

*wt*RSV A2,[54] *cpts*248/404,[55] *wt*PIV3 JS,[56] and PIV3-cp45[56] have been previously described. *cpts*248/404 contains five mutations in the biological strain derived by cold passage (cp) and the 248 and 404 temperature sensitive (*ts*) mutations were produced by exposure to 5-fluorouracil. The 404 *ts* mutation is in the gene start of the matrix M2 gene and 248 is in the L polymerase gene.[57] The growth of *cpts*248/404 is restricted at 37°C ($\geq$ 2 $\log_{10}$ pfu/mL lower than the titer at 32°C). rA2cpΔNS2 virus was derived by deleting the NS2 (interferon antagonist) gene from rA2cp.[31,58] PIV3-cp45 is a cold-adapted, *ts* virus that differs from *wt*PIV3 JS by 15

mutations.[59] bPIV3 SF is hr restricted in human cells. Recombinant bovine PIV3 SF was constructed by inserting each of the individual genes into a modified Bluescript vector (pFLII,) by RT-PCR (see Supplementary Methods online). Using modification of the protocol previously described,[60] recombinant bPIV3 SF was recovered from cDNAs. This procedure facilitates virus rescue from Vero cells without calcium phosphate precipitation or recombinant vaccinia virus helper (Witko et al, personal communication). Plasmids encoding support proteins, N, P, and L were based on PIV3-cp45 sequence rather than bPIV3 SF sequence and were the only plasmids used for the rescue in addition to those containing the full-length clones and T7 RNA polymerase. All viruses were purified by gradient ultracentrifugation described elsewhere.[60,61]

Scanning Electron Microscopy of 3D HBE TLAs

After removal from the reactor vessels, samples were washed once with calcium- and magnesium-free PBS. Day 31 to 35 samples were suspended in a buffer containing 3% glutaraldehyde and 2% paraformaldehyde in 0.1 *M* cacodylate buffer at pH 7.4[45] (Luna 1968), then rinsed for 5 minutes with cacodylate buffer three times and post-fixed with 1% osmium tetroxide (Electron Microscopy Sciences, Fort Washington, PA, USA) in cacodylate buffer for 1 hour. Samples were then rinsed three times for 5 minutes each with distilled water and then treated for 10 minutes with a Millipore (Millipore Corp., Bedford, MA, USA) (0.2-µm)-filtered, saturated solution of thiocarbohydrazide (Electron Microscopy Sciences), then washed five times for 5 minutes each with distilled water and fixed with 1% buffered osmium tetroxide for 10 minutes. This last step was necessary to prevent the microcarriers from collapsing. Samples were then rinsed with distilled water three times and dehydrated with increasing concentrations of ethanol, followed by three changes in absolute methanol. After transfer to 1,1,1,3,3,3-hexamethyldisilazane (Electron Microscopy Sciences), samples were allowed to soak for 10 minutes, drained, and air-dried overnight. Dried samples were sprinkled with a thin layer of silver paint on a specimen stub, dried, coated by vacuum evaporation with platinum-palladium alloy, and then examined in the JEOL T330 scanning electron microscopy at an accelerating voltage of 5 to 10 kV.

Transmission Electron Microscopy of 3D HBE TLAs

Day 31 to day 35 HBE TLA samples were washed three times with 0.1 M sodium cacodylate buffer pH 7.4 (#11652, Electron Microscopy Science, Port Washington, PA, USA) then fixed in a solution of 2.5% gluteraldehyde-formaldehyde in 0.1 M sodium cacodylate buffer (#15949, Electron Microscopy Science, Fort Washington, PA, USA) 0.3 M sucrose

(Sigma, St. Louis, MO, USA) – 1% DMSO (Sigma, St. Louis, MO, USA) pH 7.4 (Electron Microscopy Science, Fort Washington, PA, USA) overnight at 4°C. The fixed tissue was washed three times in 0.1 M sodium cacodylate buffer, pH 7.4 buffer, post-fixed stained in 0.1 M tannic acid (#21700, Electron Microscopy Science, Port Washington, Pa, USA) in 0.1 M sodium cacodylate pH 7.4 for 3 hours at room temperature. The tissue samples were washed three times in buffer, and then fixed again in 1.0 M osmium tetroxide (#19152, Electron Microscopy Science, Port Washington, PA, USA) in cacodylate buffer pH 7.4 for 1.5 hours at room temperature. Samples were dehydrated in a series of graded ethanol, and then embedded in EMbed - 812 resin (#14120, Electron Microscopy Science, Port Washington, PA, USA). Samples were sectioned at yellow-silver (700 A), mounted on Ni grids and examined under a JEOL JEM-1010 transmission electron microscope (JEOL, USA) at 80 kV.

Expression of epithelial markers by confocal microscopy

Normal human lung cryostat sections were obtained from BioChain Institute (Hayward, CA). 2D BEAS-2B and 2D HBTC cells were seeded onto coverslips and fixed with 4% paraformaldehyde (Electron Microscopy Sciences, Hatfield, PA, cat #15710) when 70% - 80% confluent for 30 minutes. Day 35 3D HBE TLAs were fixed in 4% paraformaldehyde for 60 minutes. All cells/tissues were incubated with the primary antibodies including EMA (Dako Cytomation, Carpinteria, CA cat #N1504), mouse anti-human cytokeratin 18, (Dako Cytomation, Carpinteria, CA cat #M7010), mouse anti-human CD54 (intercellular adhesion molecule-ICAM-1) (Dako Cytomation, Carpinteria, CA, cat #M7063, Clone 6.5B5) or mouse anti-MAP2 (Chemicon, Temecula, CA, cat #MAB3418) overnight at 4°C. Fluorescein isothiocyanate conjugated mouse anti-ZO-1 (Invitrogen – formerly Zymed, Eugene, OR, cat #33-9111) was incubated at room temperature for 2 hours. After washing five times with 1 x DPBS (Mediatech, Herndon, VA, cat #20-031-CV), the samples were incubated with the secondary antibody Alexa Fluor 555 donkey anti-mouse IgG (H + L), (Invitrogen or Molecular Probes, Eugene, OR, cat #A31570) or the Alexa Fluor 488 goat anti-mouse IgG (H + L), (Invitrogen or Molecular Probes, Eugene, OR, cat #A11029). The samples were counterstained with TO-PRO-3 iodide (Invitrogen or Molecular Probes, Eugene, OR, cat #T3605) to stain the nuclei. 3% BSA (Sigma-Aldrich, St Louis, MO, cat #A2153-50G) and 0.25% Triton (Sigma-Aldrich, St Louis, MO, cat #061K0126) in 1X PBS were used as Fc block and antibody diluents. Samples were mounted onto microscope slides using coverslips and polyvinyl alcohol (PVA, Sigma-Aldrich /Fluka, Biochemika, St Louis, MO, cat #10981) mounting medium. A Leica TCS

SL Confocal Scanner with Leica DMI RE2 inverted Microscope was used to scan all samples.

Expression of epithelial markers by immunohistochemistry

TLAs designated for histological and immunohistological staining were washed three times with gentle agitation for 5 minutes each in 1x PBS without Mg^{+2} and Ca^{+2} (Cellox Laboratories Inc, St. Paul, MN, USA) to remove foreign protein residues contributed by the growth media. The TLAs were then transferred to 50 mL polystyrene tubes containing 10% formalin buffered in PBS (Electron Microscopy Service, Ft. Washington, PA, USA). After an overnight incubation at 4°C, the fixed cells were washed three times in PBS. The TLAs were centrifuged at < 1000g to concentrate the bead-cell assembly, and 1 mL of warm noble agar was added for additional stabilization. TLAs were embedded in paraffin blocks, and thin sections were cut at 3-5 mm on a Micron HM315 microtome (Walldorf, Germany). The sections were deparaffinized by standard procedure, and the antigens were retrieved by protein kinase or citrate and blocked with a normal rabbit or mouse sera – 0.5% Tween 20 blocking solution. The antibody for mucin was used neat and the antibody for ICAM-1 was diluted 1:100 in the blocking solution and incubated on sections for 9 to 30 minutes, rinsed with distilled water and either anti-mouse, anti-goat, or anti-rabbit-conjugated horse radish peroxidase secondary antibody (Dako Envision System) was applied using an automated immunohistochemical stainer (Dako, Carpintaria, CA, USA). Slides were examined by a Zeiss Axioskop (Hamburg, Germany) microscope and images captured with a Kodak DC 290 Zoom (Rochester, NY, USA) digital camera. Brown stain indicates positive peroxidase stains for ICAM-1. Pink stain for mucin induces a positive mucicarmine stain. Immunocytochemistry of monolayer cultures were prepared as outlined previously.[9] Briefly, glass microscope slides (Rite-On, Clay Adams cat #3050) were placed in 150-mm Petri dishes (Fisher cat #25030-150). Cells were added (1x 10^3 cells/mL) and incubated at 35.5°C for 48 hours. Slides were removed and washed two times with calcium- and magnesium-free PBS (Cellos Laboratories, Inc., St. Paul, MN) and post-fixed with 10% buffered formalin (Electron Microscopy Service, Ft. Washington, PA).

Host transcriptional profiling data analysis

RNA isolation, labeling, and hybridization: Total RNA was extracted from 3D HBE TLAs (how many and what day post initiation) and BEAS-2B monolayers (how many and what day post culture initiation) with TriZol reagent (Invitrogen, Carlsbad, CA) and further purified with RNeasy mini kit (Qiagen, Valencia, CA) following the manufacturer's protocol. Integrity of the RNA was examined by electrophoresis in a 1% agarose gel, and the concentration was

determined by ultraviolet (UV) absorbance at 260 nm. Five µg of total RNA from virus- or mock-infected samples was incubated at 70°C for 10 minutes with oligo-dT containing a T7 RNA polymerase promoter sequence. The first strand cDNA was synthesized with SuperScript II for 1 hour at 50°C; the second strand with *E. coli* DNA polymerase, *E. coli* DNA ligase, and T4 DNA polymerase for 3 hours at 16°C. Double-stranded (ds) cDNA was purified with MultiScreen PCR filter plate (Millipore, Billerica, MA) and eluted with 25 µL 10mM Tris buffer. Twenty µL of eluted ds cDNA was used to synthesize cRNA for 16 hours at 37°C with T7 RNA polymerase (Epicenter, Madison, WI) and biotin-CTP/biotin-UTP (Perkin Elmer, Boston, MA). The cRNA was purified with MultiScreen PCR filter plate and quantified by UV absorbance at 260 nm. Ten µg of cRNA was fragmented and hybridized to Affymetrix HG-U133A chips according to the Affymetrix GeneChip Expression Analysis Technical Manual. In brief, cRNA was hybridized to the GeneChip for 16 hours at 45°C in a 200 µL Saline-Sodium Phosphate-EDTA buffer cocktail containing herring sperm DNA, bovine serum albumin, and a known amount of standard curve spike-in transcript pool.[62] GeneChips were stained with strepavidin-conjugated phycoerythrin (SAPE, Invitrogen, Carlsbad, CA), followed by goat biotinylated anti-strepavidin (Vector Laboratories, Burlingame, CA), and a second round of SAPE staining was performed for signal amplification. After staining, fluorescent intensity was quantified using the Affymetrix GeneChip Scanner; the array image was captured and processed into signal intensity with the Affymetrix Microarray Suite 5.0.

Data filtering, analysis, and reduction: The fluorescent intensities of all unique gene identifiers on the GeneChips were normalized based on the hybrid method of GeneChip scaled average signal (with constant mean assumption) and spike-in standard curve transcripts.[62] Unique identifiers were then filtered to those with normalized intensity higher than 10 ppm in at least two of the triplicate samples for each treatment condition. For each identifier in the filtered set, mean log-transformed expression levels for the treatment conditions were subject to analysis of variance (ANOVA) methods. To control the false discovery rate (FDR), p-values of each unique identifier were adjusted by a previously described algorithm.[63] Identifiers with FDR ≤ 0.05 and ≥ 1.95-fold change over mock-infected HBE TLAs were further analyzed for their function with the Gene Ontology tool[64] in Spotfire 8.0 (Somerville, MA) or NETAFFX web tool (Affymetrix, Santa Clara, CA).

The global functional analyses were generated through the use of Ingenuity Pathways Analysis (Ingenuity® Systems, www.ingenuity.com). The Functional Analysis identified the

biological functions and/or diseases that were most significant to the data set and were associated with biological functions and/or diseases in the Ingenuity Pathways Knowledge Base were considered for the analysis. Fischer's exact test was used to calculate a p-value determining the probability that each biological function and/or disease assigned to that data set is due to chance alone.

In vitro virus inoculation and titration

Confluent monolayer BEAS 2B and LLC-MK2 cultures were inoculated in T25 flasks with indicated viruses at multiplicity of infection (MOI) of 1. Confluent monolayer Vero cell cultures were inoculated at MOI of 0.1 since the plaquing efficiency is tenfold higher in Vero cells. The outer layer of 20-day-old 3D HBE TLAs (1- to 2-mm diameter) represent about 10% of the tri-culture. Therefore, TLAs were inoculated at a MOI of 0.1 to achieve an effective MOI of 1 for the cells on the outer surface. After virus absorption at room temperature for 1 hour, monolayers and TLA cultures were washed three times with DPBS (Invitrogen, Carlsbad, CA) and fed with media specified above. All air bubbles were removed from the RWV before rotation to eliminate shearing of the cells.[10] Approximately 65% of the culture media was replaced every 48 hours for both monolayer and TLA cultures. For virus titration, samples were collected on days 0, 2, 5, and 7 for Vero cultures, on days 0, 2, 4, 6, and 8 for LLC-MK2 and RSV-infected BEAS-2B cells, and 0, 2, 4, 6, 8, and 10 for PIV3-infected BEAS-2B and 3D HBE TLAs. For RSV titration, the entire monolayer cultures or 1 mL of the TLA cultures were flash-frozen with 1 x SPG. RSV titer was determined by immunostaining infected HEp-2 cells at 32°C as previously described. Titers of PIV3 viruses were determined in LLC-MK2 cells with medium overlay containing 0.8% agar at 32°C as previously described[65] except that plaques were visualized by an immunostain assay described previously[66] using anti-human PIV3 HN and F antibodies.

Human nasal wash samples

A clinical trial was performed to evaluate the transmission potential of PIV3-cp45 from South African vaccinees 4 to 48 months of age to seronegative playmates. In this double-blind study, subjects received 10^5 pfu of PIV3-cp45 or placebo by intranasal administration.[67] Nasal washes (20 mL) were collected on days 0, 3, 5, 7, 10, 12, 14, 17, 19, and 21 and also on any illness day. After completion of the virology analysis, a limited number of nasal wash samples were available to test for cytokine expression. Nasal wash samples from two placebos and two day 0 (samples collected right before immunization) samples from two vaccinees represent the four normal healthy controls. Nasal washes collected from two vaccinees shedding virus on day

5 and 7 and 7 and 10 represent the vaccine samples. Nasal washes collected from three subjects that developed illness from a natural *wt*PIV3 virus infection shed virus only on days 14, 17, and 19 (A); 7, 10, and 12 (B); and day 12 and 14 (C) represent *wt*PIV3 samples. Subject B had an adenovirus infection on days 0, 3, and 5 and Subject C had an enterovirus infection on day 0; however, *wt*PIV3 was the only adventitious agent detected in the samples tested for cytokines. These three subjects shedding *wt*PIV3 presented symptoms of upper respiratory tract infections, fevers, and coughs. No clinical symptoms or adventitious agents were reported for the normal healthy controls or vaccinees on the days selected for cytokine analysis.

Quantifying cytokines

Cytokine concentrations of uninfected and infected 2D and 3D culture supernatants, as well as nasal washes from healthy and PIV3-infected subjects, were determined using the Bioplex 17plex human cytokine assay kit (BioRad, Hercules CA) following the manufacturer's protocol. These cytokines include IL-2, IL-4, IL-5, IL-6, IL-7, IL-8, IL-10, IL-12 (p70), IL-13 and IL-17, TNF-α, IL-1β, MCP-1, MIP1-β, GM- CSF, G-CSF, and IFNγ. Concentrations of RANTES (Regulated upon Activation, Normal T cell-Expressed and -Secreted) and MIP-1α (Macrophage Inhibitory Factor 1-α) were determined by ELISA (R&D System, Minneapolis, MN). The supernatants analyzed represent cytokine secretion in 48-hour periods collected on day 0, 2, and 8 pi. The mean cytokine secretion concentration was determined in three experiments for MIP-1α and at least six experiments for the other cytokines. The limit of detection in the assays was 2 pg/mL for RANTES, 50 pg/mL for IL-6, G-CSF and GM-CSF, and 10 pg/mL for IL-1β, IL-2, IL4, IL-5, IL-7, IL-8, IL-10, IL-12 (p70), IL-13, IL-17, MIP-1α, MIP-1β, MCP-1, INFγ, and TNF-α. The cytokine concentrations were $\log_{10}$ transformed before analysis. Data were analyzed with Spotfire 8.0 (Spotfire Inc, Somerville, MA) to determine consistency and reproducibility. JMP 5.11 (SAS Institute Inc., Cary, NC) was used for statistical analysis. Cytokines from uninfected cells were determined to be secreted if the concentrations of >50% of the assay samples tested were above the detection limit. The fold increase of a cytokine was determined by the ratio of the mean cytokine concentration secreted from infected cultures (or nasal washes) to the corresponding mean cytokine concentration of uninfected cultures (or nasal washes). Statistical significance of cytokine levels in nasal washes in the 3D HBE TLAs and 2D BEAS- 2B cells illustrated in Table II were performed by SAS analysis.

4.0 Supplementary Methods

Construction of rbPIV3 Shipping Fever

The full-length cDNA clone of the bPIV3 SF genome was created from eight cDNA fragments of the genome, corresponding to the six genes (N, P, M, F, HN, & L) as well as the 3' leader and the 5' trailer, which were cloned separately and then joined together in one expression vector. All SF gene fragments (except L) were obtained as single fragments by RT-PCR amplification using RNA extracted from LLC-MK2 cells (ATCC Number CCL-7) infected with bovine parainfluenza virus 3, strain SF-4 (ATCC Number VR-281) as template. The individual inserts were cloned into a modified Bluescript vector (pFLII, see below), except for the SF L gene, which was amplified and cloned in three pieces into pBluescript SK+ prior to cloning into the pFLII vector. The full-length clone was created by sequentially piecing the eight fragments together using unique restriction enzyme (RE) sites that were engineered on to the ends of the cDNA fragments during RT-PCR.

The first cDNA fragment, leader, encompassed genomic nucleotides 1 through 77 and had T7 RNA polymerase promoter sequence placed directly prior to the first nucleotide, a Not I RE site upstream of the promoter, and an Age I RE site at nucleotides 72 to 77 (seven nucleotides after the N gene start signal) during RT-PCR. The second fragment, N, encompassed nucleotides 72 through 1659, overlapped the leader fragment at the Age I RE site, and contained a naturally occurring Spe I RE site at nucleotides 1654 to 1659 that embodies the N translation stop signal. The third fragment, P, encompassed nucleotides 1654 through 3594, overlapped the N fragment at the SpeI RE site, and had an engineered SalI site at nucleotides 3589 to 3594. The fourth fragment, M, encompassed nucleotides 3589 through 4831, overlapped the P fragment at the SalI RE site and had an engineered NheI RE site at nucleotides 4826 to 4831. The fifth fragment, F, encompassed nucleotides 4826 through 6701, overlapped the M fragment at the NheI RE site, and had an engineered NruI RE site at nucleotides 6695 to 6700. The sixth fragment, HN, encompassed nucleotides 6695 through 8542, overlapped the F fragment at the NruI RE site, and had an engineered RsrII RE site at nucleotides 8535 to 8541. The seventh fragment, L, once completed, encompassed nucleotides 8535 through 15371, overlapped the HN fragment the RsrII RE site, and had an engineered AvrII RE site at nucleotides 15366 to 15371. The eight fragment, trailer, encompassed nucleotides 15366 through 15456, overlapped the L fragment at the AvrII RE site, and had 26

nucleotides of a ribozyme site added downstream of the trailer with a NarI RE site after these 26 bases.

The majority of the fragments were amplified using primers of 29 to 38 nucleotides in length that matched the published bPIV3 SF sequence (GenBank Assenssion Number AF17865) at either end of the fragment except where indicated to create the RE sites mentioned above. In most cases, no more than one nucleotide was changed, but to create the RsrII site, three nucleotides were altered. The two exceptions with regard to the primer lengths were those used to amplify the start of the leader and the end of the trailer. The leader primer was 64 nucleotides in length, and, as previously described, the 5' end of that primer contained the T7 RNA polymerase promoter, sequence adjacent to the start of the bPIV3 SF genome, and a NotI site upstream of the promoter sequence (AGATATGCGGCCGCTAATACGACTCACTATAGG). The primer used to amplify the end of the trailer was 93 nucleotides in length and the 3' end contained part of the ribozyme sequence found in pFLII and the NarI site (CCAGCCGGCGCCAGCGAGGAGGCTGGGACCATGCCGGCC). The T7 promoter sequence and ribozyme where positioned so that RNA transcription with T7 and a cleavage of the RNA by the ribozyme resulted in an RNA identical to the bPIV3 SF genome.

As mentioned previously, the L gene was cloned into pBluescript SK+ in three fragments. These fragments, designated L1, L2, and L3, corresponded to genomic nucleotides 8535 through 11195, 11190 through 12969, and 12964 through 15371, respectively, and were put together to recreate L within the framework of the Bluescript plasmid sequentially using the RE sites in the following order: EagI – XbaI, XbaI – PstI, and PstI - KpnI. The XbaI and PstI RE sites are naturally occurring within the L open reading frame at nucleotide positions 11190 to 11195 and 12964 to 12969, respectively. A second XbaI RE site occurs in the L open reading frame at nucleotides 13753 to 13758 necessitating that the L3 fragment be placed into the L clone last. The EagI RE site, with an RsrII RE site seven nucleotides downstream, and the KpnI RE site, with an AvrII RE site 12 nucleotides downstream, were engineered into the cDNAs during RT-PCR for use in cloning into pBluescript. The entire L fragment was then removed from pBluescript using the RsrII and AvrII RE sites and placed into pFLII already containing the trailer fragment. The vector used as the backbone plasmid for the full-length cDNA, pFLII, was based on the previously described pFL vector used to clone full-length RSV.[60] The pFL vector was altered to remove an AgeI site that occurred seven nucleotides after the T7 terminators by digesting with AgeI RE enzyme, blunting the resultant digestion product with T4 DNA

polymerase, and re-ligating the plasmid. The pFLII multiple cloning site was introduced into pFL through PCR using the age I RE minus plasmid as the template. The pFLII multiple cloning site contains the following RE site I order Not I, Age I, Spe I, Sal I, Nhe I, Nru I, Rsr II, and Avr II.

5.0 Acknowledgments

We are grateful to Ms. L. Fasano in providing cells, V. Souza and J. Zhoa for help with the BioPlex assay, and D. DeThomas for graphics. We acknowledge the contributors to the PIV3-cp45 clinical trial, especially Drs. Peter Wright, Shabir Madhi, Jill Hackell, William Gruber, and the National Institute of Virology/National Institute for Communicable Diseases for virus culture and to the Paediatric Infectious Diseases Research Unit, Wits Health Consortium for subject recruitment. We acknowledge scientific discussions with Drs. V. Randolph, A. Thakur, and M. Pride and manuscript reviews by Drs. R. Zagursky, C. Parks, M. Hagen, D. Cooper, M. Egan, and A. Howe. We especially appreciate the work of Mr. Michael Suderman for his assistance on production of the electron micrographs.

6.0 References

[1] Collins, P.L., R.M. Chanock, and B.R. Murphy. 2001. Respiratory Syncytial Virus. *In* Fields Virology. D.M. Knipe, H. P.M., and D. Griffin, editors. 1443-1485.

[2] Cotran, R., V. Kumar, and Collins, T, Robbins. 1999. Pathologic Basis of Disease. *In* Infectious Diseases. WB Saunders Company, Philadelphia. p.347.

[3] McIntosh, K. 1991. Pathogenesis of severe acute respiratory infections in the developing world: respiratory syncytial virus and parainfluenza viruses. *Rev Infect Dis* 13 Suppl 6:S492-500.

[4] Anderson, L.J., and C.A. Heilman. 1995. Protective and disease-enhancing immune responses to respiratory syncytial virus. *J Infect Dis* 171:1-7.

[5] Shay, D.K., R.C. Holman, G.E. Roosevelt, M.J. Clarke, and L.J. Anderson. 2001. Bronchiolitis-associated mortality and estimates of respiratory syncytial virus- associated deaths among US children, 1979-1997. *J Infect Dis* 183:16-22.

[6] Welliver, R.C., D.T. Wong, M. Sun, and N. McCarthy. 1986. Parainfluenza virus bronchiolitis. Epidemiology and pathogenesis. *Am J Dis Child* 140:34-40.

[7] Glezen, W.P., Loda, F. A., and Denny, F. W. 1989. Parainfluenza viruses. *In* Viral infections of humans: epidemiology and control. A.S.e.a. Evans, editor. New York Plenum Medical Book Company, New York. 493-507.

[8] Byrd, L.G., and G.A. Prince. 1997. Animal models of respiratory syncytial virus infection. *Clin Infect Dis* 25:1363-1368.

[9] Goodwin, T.J., et al., 1993. Rotating-wall vessel coculture of small intestine as a prelude to tissue modeling: aspects of simulated microgravity. *Proc Soc Exp Biol Med* 202:181-192.

[10] Goodwin, T.J., et al.1993, Reduced shear stress: a major component in the ability of mammalian tissues to form three-dimensional assemblies in simulated microgravity. *J Cell Biochem* 51:301-311.

[11] McFadden, E.R., Jr., B.M. Pichurko, H.F. Bowman, E. Ingenito, S. Burns, N. Dowling, and J. Solway. 1985. Thermal mapping of the airways in humans. *J Appl Physiol* 58:564-570.

[12] Wright, P.F., R.A. Karron, R.B. Belshe, J. Thompson, J.E. Crowe, Jr., T.G.Boyce, L.L. Halburnt, G.W. Reed, S.S. Whitehead, E.L. Anderson, A.E. Wittek, R. Casey, M. Eichelberger, B. Thumar, V.B. Randolph, S.A. Udem, R.M. Chanock, and B.R. Murphy. 2000. Evaluation of a live, cold-passaged, temperature-sensitive, respiratory syncytial virus vaccine candidate in infancy. *J Infect Dis* 182:1331-1342.

[13] Belshe, R.B., F.K. Newman, T.F. Tsai, R.A. Karron, K. Reisinger, D. Roberton, H. Marshall, R. Schwartz, J. King, F.W. Henderson, W. Rodriguez, J.M. Severs, P.F. Wright, H. Keyserling, G.A. Weinberg, K. Bromberg, R. Loh, P. Sly, P. McIntyre, J.B. Ziegler, J. Hackell, A. Deatly, A. Georgiu, M. Paschalis, S.L. Wu, J.M. Tatem, B. Murphy, and E. Anderson. 2004. Phase 2 evaluation of parainfluenza type 3 cold passage mutant 45 live attenuated vaccine in healthy children 6-18 months old. *J Infect Dis* 189:462-470.

[14] Wright, P.F., R.A. Karron, S.A. Madhi, J.J. Treanor, J.C. King, A. O'Shea, M.R.Ikizler, Y. Zhu, P.L. Collins, C. Cutland, V.B. Randolph, A.M. Deatly, J.G. Hackell, W.C. Gruber, and B.R. Murphy. 2006. The interferon antagonist NS2 protein of respiratory syncytial virus is an important virulence determinant for humans. *J Infect Dis* 193:573-581.

[15] van Wyke Coelingh, K.L., C.C. Winter, E.L. Tierney, W.T. London, and B.R. Murphy. 1988. Attenuation of bovine parainfluenza virus type 3 in nonhuman primates and its ability to confer immunity to human parainfluenza virus type 3 challenge. *J Infect Dis* 157:655-662.

[16] Bals, R., and P.S. Hiemstra. 2004. Innate immunity in the lung: how epithelial cells fight against respiratory pathogens. *Eur Respir J* 23:327-333.

[17] Polito, A.J., and D. Proud. 1998. Epithelia cells as regulators of airway inflammation. *J Allergy Clin Immunol* 102:714-718.

[18] Garofalo, R.P., Welliver, R.C. and Ogra, P.L. 1999. Clinical Aspects of Bronchial Reactivity and Cell-Virus Interaction. *In* Mucosal Immunology. P.L. Ogra, Lamm, M. E., Bienenstock, J., Mestecky, Strobar, W. and McGhee, J. R., editor. Academic PRESS, San Diego. 1223-1237.

[19] O'Brien, L.E., M.M. Zegers, and K.E. Mostov. 2002. Opinion: Building epithelial architecture: insights from three-dimensional culture models. *Nat Rev Mol Cell Biol* 3:531-537.

[20] Knight, D.A., and S.T. Holgate. 2003. The airway epithelium: structural and functional properties in health and disease. *Respirology* 8:432-446.

[21] Gibson, M.C., and N. Perrimon. 2003. Apicobasal polarization: epithelial form and function. *Curr Opin Cell Biol* 15:747-752.

[22] Fukamachi, H., T. Mizuno, and Y.S. Kim. 1986. Morphogenesis of human colon cancer cells with fetal rat mesenchymes in organ culture. *Experientia* 42:312-315.

[23] Kaye, G.I., R.R. Pascal, and N. Lane. 1971. The colonic pericryptal fibroblast sheath: replication, migration, and cytodifferentiation of a mesenchymal cell system in adult tissue. 3. Replication and differentiation in human hyperplastic and adenomatous polyps. *Gastroenterology* 60:515-536.

[24] Buset, M., S. Winawer, and E. Friedman. 1987. Defining conditions to promote the attachment of adult human colonic epithelial cells. *In Vitro Cell Dev Biol* 23:403-412.

[25] Daneker, G.W., Jr., A.M. Mercurio, L. Guerra, B. Wolf, R.R. Salem, D.J. Bagli, and G.D. Steele, Jr. 1987. Laminin expression in colorectal carcinomas varying in degree of differentiation. *Arch Surg* 122:1470-1474.

[26] Durban, E.M. 1990. Mouse submandibular salivary epithelial cell growth and differentiation in long-term culture: influence of the extracellular matrix. *In Vitro Cell Dev Biol* 26:33-43.

[27] Garofalo, R.P., and H. Haeberle. 2000. Epithelial regulation of innate immunity to respiratory syncytial virus. *Am J Respir Cell Mol Biol* 23:581-585.

[28] Whitehead, S.S., C.Y. Firestone, R.A. Karron, J.E. Crowe, Jr., W.R. Elkins, P.L. Collins, and B.R. Murphy. 1999. Addition of a missense mutation present in the L gene of respiratory syncytial virus (RSV) cpts530/1030 to RSV vaccine candidate cpts248/404 increases its attenuation and temperature sensitivity. *J Virol* 73:871-877.

[29] Crowe, J.E., Jr., P.T. Bui, G.R. Siber, W.R. Elkins, R.M. Chanock, and B.R. Murphy. 1995. Cold-passaged, temperature-sensitive mutants of human respiratory syncytial virus (RSV) are highly attenuated, immunogenic, and protective in seronegative chimpanzees, even when RSV antibodies are infused shortly before immunization. *Vaccine* 13:847-855.

[30] Karron, R.A., P.F. Wright, R.B. Belshe, B. Thumar, R. Casey, F. Newman, F.P. Polack, V.B. Randolph, A. Deatly, J. Hackell, W. Gruber, B.R. Murphy, and P.L. Collins. 2005. Identification of a recombinant live attenuated respiratory syncytial virus vaccine candidate that is highly attenuated in infants. *J Infect Dis* 191:1093-1104.

[31] Whitehead, S.S., A. Bukreyev, M.N. Teng, C.Y. Firestone, M. St Claire, W.R. Elkins, P.L. Collins, and B.R. Murphy. 1999. Recombinant respiratory syncytial virus bearing a deletion of either the NS2 or SH gene is attenuated in chimpanzees. *J Virol* 73:3438-3442.

[32] Unsworth, B.R., Lelkes, P.I. 2000. Tissue Assembly in Microgravity. *In* Principles of Tissue Engineering. R.P. Lanza, Langer, R, Vacanti, J.P., editor. Academic Press. 157-164.

[33] Zhang, L., M.E. Peeples, R.C. Boucher, P.L. Collins, and R.J. Pickles. 2002. Respiratory syncytial virus infection of human airway epithelial cells is polarized, specific to ciliated cells, and without obvious cytopathology. *J Virol* 76:5654-5666.

[34] Carterson, A.J., K. Honer zu Bentrup, C.M. Ott, M.S. Clarke, D.L. Pierson, C.R. Vanderburg, K.L. Buchanan, C.A. Nickerson, and M.J. Schurr. 2005. A549 lung epithelial cells grown as three-dimensional aggregates: alternative tissue culture model for Pseudomonas aeruginosa pathogenesis. *Infect Immun* 73:1129-1140.

[35] MacDonald, N.E., C.B. Hall, S.C. Suffin, C. Alexson, P.J. Harris, and J.A. Manning. 1982. Respiratory syncytial viral infection in infants with congenital heart disease. *N Engl J Med* 307:397-400.

[36] Karron, R.A., P.F. Wright, S.L. Hall, M. Makhene, J. Thompson, B.A. Burns, S. Tollefson, M.C. Steinhoff, M.H. Wilson, D.O. Harris, and et al. 1995. A live attenuated bovine parainfluenza virus type 3 vaccine is safe, infectious, immunogenic, and phenotypically stable in infants and children. *J Infect Dis* 171:1107-1114.

[37] Wright, P.F., M.R. Ikizler, R.A. Gonzales, K.N. Carroll, J.E. Johnson, and J.A. Werkhaven. 2005. Growth of respiratory syncytial virus in primary epithelial cells from the human respiratory tract. *J Virol* 79:8651-8654.

[38] McNamara, P.S., and R.L. Smyth. 2002. The pathogenesis of respiratory syncytial virus disease in childhood. *Br Med Bull* 61:13-28.

[39] Noah, T.L., F.W. Henderson, I.A. Wortman, R.B. Devlin, J. Handy, H.S. Koren, and S. Becker. 1995. Nasal cytokine production in viral acute upper respiratory infection of childhood. *J Infect Dis* 171:584-592.

[40] Welliver, R.C. 2003. Respiratory syncytial virus and other respiratory viruses. *Pediatr Infect Dis J* 22:S6-10; discussion S10-12.

[41] Bonville, C.A., H.F. Rosenberg, and J.B. Domachowske. 1999. Macrophage inflammatory protein-1alpha and RANTES are present in nasal secretions during ongoing upper respiratory tract infection. *Pediatr Allergy Immunol* 10:39-44.

[42] Sheeran, P., H. Jafri, C. Carubelli, J. Saavedra, C. Johnson, K. Krisher, P.J.Sanchez, and O. Ramilo. 1999. Elevated cytokine concentrations in the nasopharyngeal and tracheal secretions of children with respiratory syncytial virus disease. *Pediatr Infect Dis J* 18:115-122.

[43] 2003. The Cytokine Handbook. Academic Press. 1536 pp.

[44] Gern, J.E., M.S. Martin, K.A. Anklam, K. Shen, K.A. Roberg, K.T. Carlson- Dakes, K. Adler, S. Gilbertson-White, R. Hamilton, P.A. Shult, C.J. Kirk, D.F. Da Silva, S.A. Sund, M.R. Kosorok, and R.F. Lemanske, Jr. 2002. Relationships among specific viral pathogens, virus-induced interleukin-8, and respiratory symptoms in infancy. *Pediatr Allergy Immunol* 13:386-393.

[45] Harrison, A.M., C.A. Bonville, H.F. Rosenberg, and J.B. Domachowske. 1999. Respiratory syncytical virus-induced chemokine expression in the lower airways:eosinophil recruitment and degranulation. *Am J Respir Crit Care Med* 159:1918-1924.

[46] Garofalo, R.P., J. Patti, K.A. Hintz, V. Hill, P.L. Ogra, and R.C. Welliver. 2001.Macrophage inflammatory protein-1alpha (not T helper type 2 cytokines) is associated with severe forms of respiratory syncytial virus bronchiolitis. *J Infect Dis* 184:393-399.

[47] Noah, T.L., and S. Becker. 2000. Chemokines in nasal secretions of normal adults experimentally infected with respiratory syncytial virus. *Clin Immunol* 97:43-49.

[48] Tripp, R.A. 2004. Pathogenesis of respiratory syncytial virus infection. *Viral Immunol* 17:165-181.

[49] McNamara, P.S., B.F. Flanagan, C.A. Hart, and R.L. Smyth. 2005. Production of chemokines in the lungs of infants with severe respiratory syncytial virus bronchiolitis. *J Infect Dis* 191:1225-1232.

[50] Mejias, A., S. Chavez-Bueno, and O. Ramilo. 2005. Respiratory syncytial virus pneumonia: mechanisms of inflammation and prolonged airway hyperresponsiveness. *Curr Opin Infect Dis* 18:199-204.

[51] Wang, S.Z., and K.D. Forsyth. 2000. The interaction of neutrophils with respiratory epithelial cells in viral infection. *Respirology* 5:1-10.

[52] McNamara, P.S., P. Ritson, A. Selby, C.A. Hart, and R.L. Smyth. 2003.Bronchoalveolar lavage cellularity in infants with severe respiratory syncytial virus bronchiolitis. *Arch Dis Child* 88:922-926.

[53] Ke, Y., R.R. Reddel, B.I. Gerwin, M. Miyashita, M. McMenamin, J.F. Lechner, and C.C. Harris. 1988. Human bronchial epithelial cells with integrated SV40 virus T antigen genes retain the ability to undergo squamous differentiation. *Differentiation* 38:60-66.

[54] Lewis, F.A., Rae, M.L., Lehman, N.I., and Ferris, A.A. 1961. A syncytial virus associated with epidemic disease of the lower respiratory tract in infants and young children. *Med. J. Aust.* 2:932-933.

[55] Crowe, J.E., Jr., P.T. Bui, A.R. Davis, R.M. Chanock, and B.R. Murphy. 1994. A further attenuated derivative of a cold-passaged temperature-sensitive mutant of human respiratory syncytial virus retains immunogenicity and protective efficacy against wild-type challenge in seronegative chimpanzees. *Vaccine* 12:783-790.

[56] Belshe, R.B., and F.K. Hissom. 1982. Cold adaptation of parainfluenza virus type 3: induction of three phenotypic markers. *J Med Virol* 10:235-242.

[57] Whitehead, S.S., C.Y. Firestone, P.L. Collins, and B.R. Murphy. 1998. A single nucleotide substitution in the transcription start signal of the M2 gene of respiratory syncytial virus vaccine candidate cpts248/404 is the major determinant of the temperature-sensitive and attenuation phenotypes. *Virology* 247:232-239.

[58] Whitehead, S.S., K. Juhasz, C.Y. Firestone, P.L. Collins, and B.R. Murphy. 1998. Recombinant respiratory syncytial virus (RSV) bearing a set of mutations from cold-passaged RSV is attenuated in chimpanzees. *J Virol* 72:4467-4471.

[59] Skiadopoulos, M.H., S. Surman, J.M. Tatem, M. Paschalis, S.L. Wu, S.A. Udem, A.P. Durbin, P.L. Collins, and B.R. Murphy. 1999. Identification of mutations contributing to the temperature-sensitive, cold-adapted, and attenuation phenotypes of the live-attenuated cold-passage 45 (cp45) human parainfluenza virus 3 candidate vaccine. *J Virol* 73:1374-1381.

[60] Elliott, M.B., K.S. Pryharski, Q. Yu, C.L. Parks, T.S. Laughlin, C.K. Gupta, R.A. Lerch, V.B. Randolph, N.A. LaPierre, K.M. Dack, and G.E. Hancock. 2004. Recombinant respiratory syncytial viruses lacking the C-terminal third of the attachment (G) protein are immunogenic and attenuated in vivo and in vitro. *J Virol* 78:5773-5783.

[61] Sanchez, A., and A.K. Banerjee. 1985. Studies on human parainfluenza virus 3: characterization of the structural proteins and in vitro synthesized proteins coded by mRNAs isolated from infected cells. *Virology* 143:45-54.

[62] Hill, A.A., E.L. Brown, M.Z. Whitley, G. Tucker-Kellogg, C.P. Hunter, and D.K. Slonim. 2001. Evaluation of normalization procedures for oligonucleotide array data based on spiked cRNA controls. *Genome Biol* 2:RESEARCH0055.

[63] Reiner, A., D. Yekutieli, and Y. Benjamini. 2003. Identifying differentially expressed genes using false discovery rate controlling procedures. *Bioinformatics* 19:368-375.

[64] Ashburner, M., C.A. Ball, J.A. Blake, D. Botstein, H. Butler, J.M. Cherry, A.P. Davis, K. Dolinski, S.S. Dwight, J.T. Eppig, M.A. Harris, D.P. Hill, L. Issel- Tarver, A. Kasarskis, S. Lewis, J.C. Matese, J.E. Richardson, M. Ringwald, G.M. Rubin, and G. Sherlock. 2000. Gene ontology: tool for the unification of biology. The Gene Ontology Consortium. *Nat Genet* 25:25-29.

[65] Karron, R.A., P.F. Wright, F.K. Newman, M. Makhene, J. Thompson, R. Samorodin, M.H. Wilson, E.L. Anderson, M.L. Clements, B.R. Murphy, and et al.1995. A live human parainfluenza type 3 virus vaccine is attenuated and immunogenic in healthy infants and children. *J Infect Dis* 172:1445-1450.

[66] Randolph, V.B., M. Kandis, P. Stemler-Higgins, M.S. Kennelly, Y.M. McMullen, D.J. Speelman, and C. Weeks-Levy. 1994. Attenuated temperature-sensitive respiratory syncytial virus mutants generated by cold adaptation. *Virus Res* 33:241-259.

[67] Madhi, S.A., C. Cutland, Y. Zhu, J.G. Hackell, F. Newman, N. Blackburn, B.R. Murphy, R.B. Belshe, R.A. Karron, A.M. Deatly, W.C. Gruber, D.I. Bernstein, and P.F. Wright. 2006. Transmissibility, infectivity and immunogenicity of a live human parainfluenza type 3 virus vaccine (HPIV3cp45) among susceptible infants and toddlers. *Vaccine* 24:2432-2439.

REPORT DOCUMENTATION PAGE

Form Approved
OMB No. 0704-0188

1. AGENCY USE ONLY *(Leave Blank)*	2. REPORT DATE	3. REPORT TYPE AND DATES COVERED
	August 2012	NASA Technical Paper

4. TITLE AND SUBTITLE
Paramyxovirus Infection Mimics In Vivo Cellular Dynamics in Three-Dimensional Human Bronchio-Epithelial Tissue-Like Assemblies

5. FUNDING NUMBERS

6. AUTHOR(S)
Anne M. Deatly, Yen-Huei Lin, Maureen McCarthy, Wei Chen, Lynn Z. Miller, Jorge Quiroz, Becky M. Nowak, Robert A. Lerch, Stephen A. Udem, Thomas J. Goodwin

7. PERFORMING ORGANIZATION NAME(S) AND ADDRESS(ES)
Lyndon B. Johnson Space Center
Houston, Texas 77058

8. PERFORMING ORGANIZATION REPORT NUMBERS
S-1125

9. SPONSORING/MONITORING AGENCY NAME(S) AND ADDRESS(ES)
National Aeronautics and Space Administration
Washington, DC 20546-0001

10. SPONSORING/MONITORING AGENCY REPORT NUMBER
TP-2012-217363

11. SUPPLEMENTARY NOTES

12a. DISTRIBUTION/AVAILABILITY STATEMENT
Available from the NASA Center for AeroSpace Information (CASI)
7121 Standard
Hanover, MD 21076-1320 Category: 52

12b. DISTRIBUTION CODE

13. ABSTRACT *(Maximum 200 words)*
Respiratory syncytial virus and parainfluenza virus cause severe respiratory disease, especially in infants, children, and the elderly. An in vitro model that accurately mimics infection of the human respiratory epithelium would facilitate vaccine development greatly. Monolayer cultures traditionally used to study these viruses do not accurately and precisely differentiate the replication efficiencies of wild type and attenuated viruses. Therefore, we engineered novel three-dimensional tissue-like assemblies of human bronchio-epithelial cells to produce a more physiologically relevant in vitro model of the human respiratory epithelium. Tissue-like assemblies resemble human respiratory epithelium structurally and by expression of differentiated epithelial cell markers. Most significantly, wild type viruses exhibited a clear growth advantage over attenuated strains in tissue-like assemblies unlike monolayer cultures. In addition, the tissue-like assemblies responded to virus infection by secreting pro-inflammatory mediators similar to the respiratory epithelia of infected children. These characteristics make the tissue-like assembly model a valuable platform technology to develop and evaluate live, attenuated respiratory virus vaccine candidates for human use.

14. SUBJECT TERMS	15. NUMBER OF PAGES	16. PRICE CODE
in vitro methods and tests; viruses; 3D in vitro human respiratory epithelia, respiratory syncytial virus, parainfluenza virus type 3, virus attenuation, cytokine profile	42	

17. SECURITY CLASSIFICATION OF REPORT	18. SECURITY CLASSIFICATION OF THIS PAGE	19. SECURITY CLASSIFICATION OF ABSTRACT	20. LIMITATION OF ABSTRACT
Unclassified	Unclassified	Unclassified	Unlimited